Ain Shams Engineering Journal xxx (xxxx) xxx

Contents lists available at ScienceDirect

Ain Shams Engineering Journal

journal homepage: https://www.sciencedirect.com

Full Length Article

MILP-MPC for planned maneuver station-keeping and collision avoidance of GEO satellites using on-off chemical thrusters

Mohamed Karim [a,*], Mohamed Ibrahim [a], Hosam Hendy [b], Mahmoud Ashry [c], Yehia Z. Elhalwagy [d]

[a] Automatic Control Systems Department, Military Technical College (MTC), Cairo, Egypt
[b] Director of Space Engineering Research Center, Military Technical College (MTC), Cairo, Egypt
[c] Arab Academy for Science, Technology and Maritime Transport (AAST), Giza, Egypt
[d] Vice Dean, Faculty of Engineering, Modern Sciences & Arts University (MSA), Giza, Egypt

ARTICLE INFO

Keywords:
Geostationary Earth orbit (GEO)
Station-keeping
Mixed integer linear programming (MILP)
Model predictive control (MPC)

ABSTRACT

GEO satellites require precise station-keeping and ensuring collision avoidance to maintain their desired orbital positions and ensure uninterrupted communication services. However, maneuvering these satellites poses significant challenges due to various geophysical factors and orbital perturbations. This work proposes a model predictive control for planned maneuver station-keeping and collision avoidance of GEO satellites using south, east, and west maneuvers. These maneuvers have been achieved using on/off chemical thrusters with a short firing time. The station-keeping problem is reformulated as an optimization problem using mixed-integer linear programming. MILP-MPC formulation simultaneously considers multiple objectives and constraints such as fuel consumption, maneuver planning, and collision avoidance for mitigating collision risks. Simulation results demonstrate the effectiveness of the proposed MILP-MPC framework compared to the real-time telemetry in achieving accurate station-keeping and collision-free operation while optimizing fuel consumption. The proposed controller increases the satellite lifetime by reducing the thruster firing time.

1. Introduction

Satellites in geostationary Earth orbit (GEO) play a critical role in various applications, e.g., communication, broadcasting, and weather monitoring. To achieve these missions, GEO satellites travel around the Earth on a GEO orbit of approximately 36,000 km to cover about a third of the planet while appearing stationary from the surface of the Earth. Therefore, precise station-keeping and reliable maneuvering are crucial for accurately maintaining the desired orbital positions over a fixed Earth location. For instance, station-keeping ensures that the satellite remains in its assigned orbital slot, providing uninterrupted communication services.

For more space exploration, the management of GEO satellites requires advanced methodologies for precise station-keeping and collision-avoidance maneuvers. Therefore, GEO satellites require precise control mechanisms to maintain their designated orbital positions despite various perturbation forces, e.g., non-Keplerian and solar radiation pressure, as well as Earth and lunar gravitational fields. These perturbations might cause the orbit to deviate [1].

However, the other challenges are due to controlled and uncontrolled space objects, e.g., newly launched satellites, collision debris, and rocket bodies [2,3]. Thus, they increase the failure risk of all spacecraft in orbit. Currently, more than 27,000 fragments of space debris are being monitored. For instance, the 2009 Iridium-Cosmos collision fragmented approximately 1850 debris pieces that were greater than ten cm in size [4]. Therefore, it is necessary to implement precise station-keeping and preemptive collision avoidance strategies to safeguard the operational integrity of satellites. So, satellite control centers are compelled to maintain heightened situational awareness to promptly enact unplanned collision avoidance maneuvers [5,6].

Therefore, various station-keeping maneuvers are regularly planned to ensure GEO satellites remain within predefined windows, i.e., orbital

* Corresponding author.
E-mail addresses: kareem.ashraf@hotmail.com (M. Karim), mohamed.ibrahim@mtc.edu.eg (M. Ibrahim), h.hendy@mtu.edu.eg (H. Hendy), mmaashry@aast.edu (M. Ashry), yelhalwagy@msa.edu.eg (Y.Z. Elhalwagy).
URL: http://www.mtc.edu.eg/mtcwebsite/ (M. Ibrahim).

https://doi.org/10.1016/j.asej.2024.103145
Received 12 March 2024; Received in revised form 5 October 2024; Accepted 2 November 2024

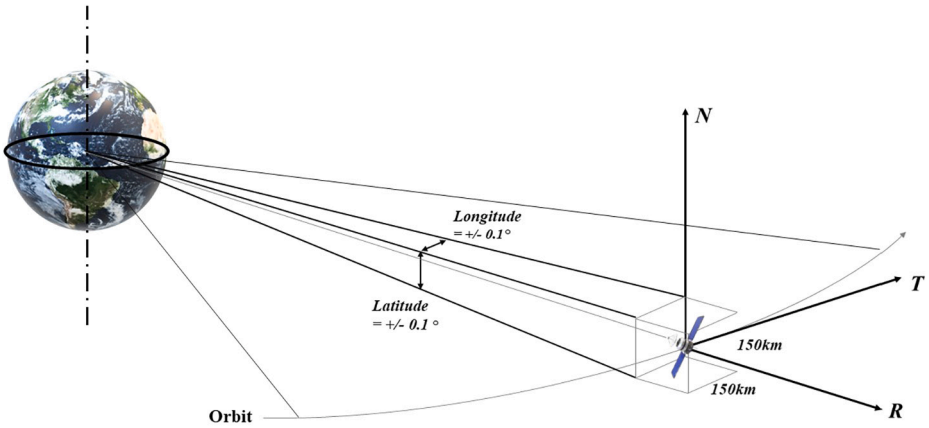

Fig. 1. Satellite position in the station-keeping box typically around ±0.01° latitude/longitude.

slots, while concurrently aligning their antennas with prescribed footprints. For instance, the south/north maneuver adjusts inclination, while the east/west maneuver adjusts the semi-major axis and eccentricity. Failure to execute these adjustments might cause deviations from the assigned orbital slots, leading the satellite to move out of the station-keeping box, see Fig. 1. This box is a designated region within GEO orbit, where the satellite must remain to fulfill its operational objectives [7].

1.1. State of the art

Various methodologies have been proposed to enhance the station-keeping strategies of GEO satellites, considering distinct aspects of orbit control and fuel optimization. For instance, a daily north/south station-keeping technique [7] was tailored for GEO satellites to mitigate drift accumulation and minimize inclination oscillation periods. A hierarchical fuzzy-optimal controller [8] was proposed for station-keeping maneuver under different environmental accelerations. The fuzzy control system is used to turn on thrusters while a genetic optimization algorithm determines the duty cycle of each thruster. A multi-objective genetic algorithm [9] was employed for optimal collision avoidance maneuvers under various operational constraints using less fuel than standard orbit control procedures.

The collision avoidance problem was formulated as a convex optimization in [10] to determine the fuel-optimal paths in space despite the system uncertainty. Another work [11] used primal-dual interior-point algorithms to solve convex optimization problems for collision avoidance maneuvers. The optimizer successfully yields optimal solutions across all test cases, even without prior knowledge of thrust arc structure or direction. A sequential convex program in [12] was devised for fuel-efficient collision avoidance maneuvers using diverse dynamical models. Thus, it incorporated high-order gravitational harmonics, atmospheric drag, and solar radiation pressure. Another collision avoidance controller [13] used reinforcement learning based on proximal policy optimization that includes collision probability and energy consumption. Thus, it learns from motion states and extracts information about hazards to determine decisions for steering away from dangerous areas.

However, most of the proposed approaches in the literature have not considered the satellite model and constraints, e.g., thruster operational limits. Thus, it might lead to infeasible maneuvers. So these approaches may struggle to simultaneously handle complex maneuvers, fuel constraints, and the discrete nature of on-off chemical thrusters. Furthermore, it is required to optimize propellant consumption and ensure precise station-keeping. Therefore, several model predictive controllers (MPC) were proposed to execute various objectives, e.g., station-keeping and energy consumption, while considering the satellite model and constraints. MPC utilizes a predictive model of the system to optimize future control inputs over a finite horizon, considering constraints and objectives. For instance, an MPC approach [14] was proposed for executing station-keeping, attitude control, and momentum management for a GEO satellite. This MPC approach was used with an on/off quantization scheme to determine a continuous thrust command quantized as a single on/off pulse. So MPC utilized significantly fewer on-off pulses than alternative approaches, e.g., pulse width modulation [15].

Another MPC approach [16] used a prediction model of environmental disturbance forces for low-thrust satellites. This policy effectively adheres to the specified constraints while minimizing fuel consumption comparable to that of meticulously designed open-loop maneuvers. A more recent MPC framework [1] achieved the station-keeping objective with minimum velocity increments based on model of the relative orbital elements. A convex optimization-based MPC strategy was introduced in [17] to guide active debris removal missions with minimum fuel consumption. Another MPC system [18] employs the Hammerstein model for a three-axis gimbal used in target tracking to improve its robustness against external disturbances. The system's nonlinearity was captured by identifying a simplified input-output model using the nonlinear Hammerstein model structure and the Output Error (OE) approach.

Split-prediction-horizon MPC [19] was proposed for station-keeping and attitude control of GEO satellites. In this setup, two prediction split horizons were used, a shorter one for the orbital inclination and a longer one for all other states. This policy required a delta velocity much smaller than a single-horizon approach, so the MPC policy reduced the overall number of on-off pulses and, thereby, fuel consumption. Later, this MPC approach [19] was validated through a closed-loop simulation using the high-precision orbit propagation systems tool-kit (STK) in [20].

Many GEO satellites utilize on/off propulsion systems for orbital adjustments to minimize energy consumption. However, existing MPC approaches for GEO satellites often rely on continuous control inputs or do not explicitly consider the discrete natural of the chemical thrusters. This paper addresses these limitations by proposing a novel MILP-MPC framework that incorporates both continuous and discrete variables, allowing for the efficient handling of on-off thrusters and collision avoidance requirements. Thus, it requires reformulating the station-keeping problem as mixed integer linear programming (MILP), e.g., in [21–23]. Thus, MILP allows the incorporation of continuous variables, e.g., velocity and attitude, with other integer decision variables, e.g., switching on/off the thrusters. For instance, the optimized station-keeping strategy [21] was established by analyzing the physical effects of disturbing forces on the satellite for a time horizon of one week. However, transforming the station-keeping problem into a MILP faces numerical challenges, especially over a long-term horizon, e.g., one year [22]. This issue was solved by dissecting the station-keeping problem into three consecutive control problems. Therefore, the long-term horizon was divided into several shorter control cycles, e.g., one week [23]. While some studies have been on using MILP for satellite control, their fo-

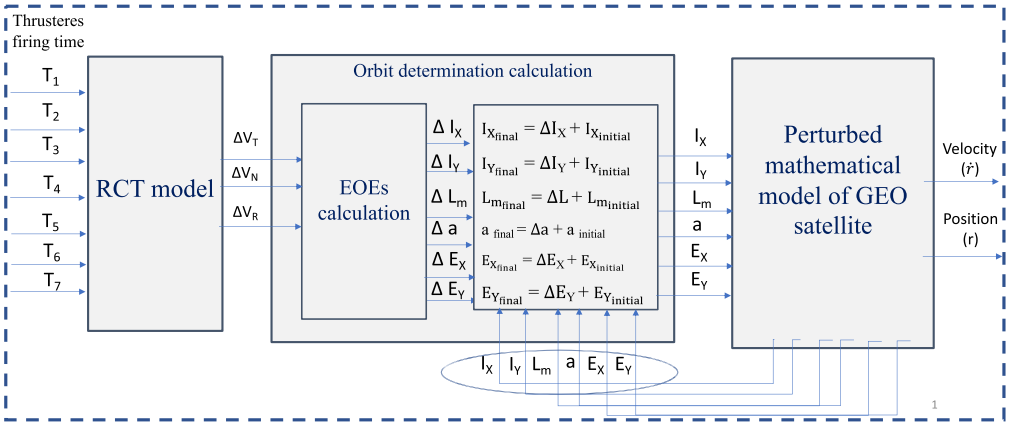

Fig. 2. Block Diagram of the Orbit Correction Model: The figure illustrates the three-block system used for GEO satellite orbit control. The model includes the Reaction Control Thruster (RCT) block, an orbit determination block that updates the Equinoctial Orbital Elements (EOEs), and the SDP4 propagator block, which accounts for geophysical perturbations to predict the satellite's updated position and velocity.

cus has primarily been on trajectory optimization and mission planning. This paper extends the application of MILP to the real-time control of GEO satellites, demonstrating its effectiveness for station-keeping and collision avoidance.

1.2. Work contribution, novelty, and structure

Traditional control techniques often face challenges in handling complex maneuvers, fuel constraints, and the discrete nature of on-off chemical thrusters. To address these issues, this work introduces a novel MILP-MPC approach to simultaneously achieve station-keeping and collision-avoidance maneuvers. MILP offers a powerful tool for solving optimization problems with continuous and discrete variables. Incorporating MILP-MPC offers a powerful framework for optimizing satellite trajectories and fuel consumption. The proposed approach leverages the capabilities of on-off chemical thrusters to improve the stability of satellite operations. For instance, the proposed controller incorporates different durations, i.e., firing time, of each thruster on the optimization problem. This leads to optimal usage of all thrusters, achieving precise tracking with minimum firing time by continuously monitoring satellite behavior and adjusting control inputs in real-time. This work provides an in-depth exploration of the design and implementation of MILP-MPC for station-keeping missions. For instance, different weights have been used for various maneuvers, e.g., east/west or south/north. These methods offer precision and efficiency in planned maneuvers, making them essential tools for longer satellite operations in orbit. So, combining MILP and MPC optimizes fuel consumption using chemical thrusters with short firing times. Moreover, this article explores the unique challenges faced by GEO satellites, performance evaluation, and comparative analysis with traditional techniques. The article also discusses potential future enhancements and applications of MPC in the station-keeping of GEO satellites.

This article is structured as follows. Section 2 presents an overview of the dynamics of satellite motion and chemical thruster positions. MILP-based MPC setup for station-keeping is illustrated in Section 3. Section 4 delves into the definitions of planned station-keeping and collision avoidance maneuver strategies. Then we elaborate on the proposed model simulation, implementation details, and comparative analyses with real-world cases to validate the proposed methodology. Lastly, Section 5 concludes the proposed study with some future perspectives.

2. Station-keeping problem setup

Station-keeping refers to continuously adjusting a satellite's position to counteract the effects of various perturbing forces. Without proper station-keeping, satellites would drift from their assigned positions, leading to signal disruptions and significant issues in satellite communication. The gravitational forces and orbital perturbations require meticulous planning and precise execution to keep satellites locked in their designated positions with minimal drift. Therefore, GEO satellites require precise and efficient control mechanisms to maintain their designated orbital positions despite these perturbations with minimum fuel consumption to extend the satellite's operational lifespan. This Section outlines the perturbed mathematical model of GEO satellites, which encompasses the calculations of the equinoctial orbital elements and the correction maneuvers by defining the orbital elements in the reference coordinate frames.

2.1. Orbit correction mathematical model

The mathematical model comprises three primary blocks, as illustrated in Fig. 2. The first block is the Reaction Control Thruster (RCT) model, which takes thruster firing time as input. Its primary function is to calculate the delta velocity ($\Delta\mathcal{V}$) in the normal, tangential, and radial directions for all thrusters by integrating the resultant acceleration generated during thruster firing.

The output $\Delta\mathcal{V}$ of our RCT model, which has been implemented and validated in [24], serves as input to the second block. This block is an orbit-determination model that computes the rate of change of the Equinoctial-Orbital-Elements (EOEs) due to the thruster firings. These rates of change are then added to the initial EOEs (prior to the thruster firings) to obtain the updated EOEs.

The updated EOEs, generated by the orbit determination model that has also been implemented and validated in [25], serve as the input to the third block, which is the perturbed mathematical model of the GEO satellite. This model is implemented using the widely employed SDP4 propagator, which is essential for predicting satellite positions in orbit determination and propagation tasks. For deep-space satellites, SDP4 incorporates equations considering the geophysical factors that affect the GEO satellites like gravitational pulls of both the Moon and Sun, solar radiation pressure effect and Earth gravity harmonics, e.g., sectoral and tesseral [26]. The final output of this block is the updated position and velocity of the satellite.

2.2. Geophysical factors and orbital perturbations in GEO satellites

GEO satellites are influenced by three primary geophysical factors, or orbital perturbing forces: solar radiation pressure, the non-spherical gravitational field of the Earth, and the gravitational effects of the Moon and the Sun (luni-solar gravity).gradient [1,8]. For instance, non-Keplerian perturbation forces cause the satellite to deviate from its intended orbital location. Understanding and compensating for these

factors is crucial for maintaining the satellite in its correct orbital position and ensuring its proper functioning over its operational lifetime.

2.2.1. Solar radiation pressure

The force exerted by sunlight on the satellite's surface can cause small but continuous changes in the satellite's orbit, particularly in its eccentricity and semi-major axis [1]. The acceleration induced by solar radiation pressure can be computed as [8]:

$$\mathbb{a}_{\rho solar} = \mathbb{C}_{\mathbb{R}} \cdot \rho_o \cdot \frac{\mathbb{A}}{m} \cdot (\mathbb{A}\upsilon)^2 \cdot \frac{r_{s\mathbb{S}}}{\|r_{s\mathbb{S}}\|^3}. \tag{1}$$

Herein m is the satellite mass, and $\mathbb{A}$ is the surface area perpendicular to the Sun radiation. $\mathbb{C}_{\mathbb{R}} = 1 + \epsilon$ is the radiation pressure coefficient and $\rho_o \approx 4.56 \times 10^{-6} N m^{-2}$ is the solar radiation coefficient. For conventional materials utilized in satellite construction, the reflectivity (ϵ) typically ranges from 0.2 to 0.9. The astronomical unit ($\mathbb{A}\upsilon$) is equal to 149.6 million km from the Sun, and the magnitude of the position vector of the Sun to the satellite is $r_{s\mathbb{S}}$ [8].

2.2.2. Non-spherical Earth gravitational field

The non-spherical gravitational field of the Earth affects orbit eccentricity and semi-major axis [1]. For instance, Earth's gravitational effect in the environmental potential function $\mu(d, \zeta, \vartheta)$ is expressed by using spherical coordinates (d, ζ, ϑ) [8]

$$\mu(d,\zeta,\vartheta) = \frac{\mathbb{GM}_{\mathbb{E}}}{d} \sum_{i=0}^{\infty} \sum_{j=0}^{i} \frac{R_{eq}}{(d)^n} \times \rho_{ij} sin(\vartheta) \times [c_{ij} cos(j\zeta) + s_{ij} sin(j\zeta)] \tag{2}$$

Herein, d is the distance from the Earth's center. R_{eq} and $\mathbb{GM}_{\mathbb{E}}$ are the mean equatorial radius and gravitational constant of the Earth. The geocentric longitude and latitude are given by ζ and ϑ, respectively. The harmonic coefficients are c_{ij} and s_{ij}. The Legendre polynomials are $\rho_{ij} sin(\vartheta)$.

2.2.3. Luni-solar gravity gradient

The gravitational pull from the Moon and the Sun can cause perturbations in the satellite's orbit, affecting its stability and requiring adjustments. The solar and lunar gravitational perturbations can be conceptualized as third-body forces that cause drift in orbital inclination and the gravitational acceleration [8]:

$$\mathbb{a}_{\mathbb{SM}} = \mathbb{GM}_{\mathbb{S}} \frac{(r_{\mathbb{S}} - r)}{|(r_{\mathbb{S}} - r)|^3} - \frac{r_{\mathbb{S}}}{|r_{\mathbb{S}}|^3} + \mathbb{GM}_{\mathbb{M}} \frac{(r_{\mathbb{M}} - r)}{|(r_{\mathbb{M}} - r)|^3} - \frac{r_{\mathbb{M}}}{|r_{\mathbb{M}}|^3} \tag{3}$$

where the gravitational coefficients of the Sun and the Moon are $\mathbb{GM}_{\mathbb{S}}$ and $\mathbb{GM}_{\mathbb{M}}$, and the position vectors of the satellite, the Sun, and the Moon are r, $r_{\mathbb{S}}$, and $r_{\mathbb{M}}$, respectively [8].

2.3. Thrusters positioning and forces

The positioning of the chemical thrusters on a satellite plays a crucial role in ensuring its proper functioning and maneuverability in space as well as orbital corrections using the available force directions. In this work, seven chemical thrusters are placed at strategic locations across the satellite body. Thus they change its orientation, adjust its trajectory, and execute complicated maneuvers, e.g., orbit insertion or station-keeping, see Fig. 3. Therefore, the precise placement of these thrusters should meticulously consider various factors, e.g., weight distribution, symmetry, and propellant efficiency. For instance, the first three thrusters are located for executing $\Delta\mathbb{V}_n$ (normal), primarily facilitating the south maneuver. Thrusters four and five are tasked with executing $\Delta\mathbb{V}_\tau$ (tangential) for the adjustments of the east and the west maneuvers, respectively. Lastly, thrusters six and seven are responsible for $\Delta\mathbb{V}_r$ (radial), primarily for attitude control during maneuvers [24].

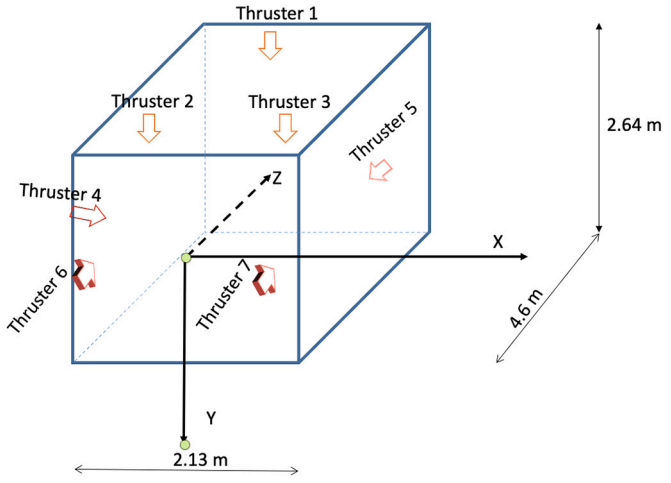

Fig. 3. The configuration of the seven thrusters allows the force to be exerted in the +X direction by thruster number four, -X direction by thruster number five, +Y direction by thrusters one, two, and three, and +Z direction by thrusters six and seven.

2.3.1. Propulsive force

In station-keeping mode, the satellite uses on-off chemical thrusters as actuators to control its position, correct deviations from orbit, and avoid potential collisions. In this work, seven on-off chemical thrusters provide the necessary propulsion to adjust satellite orbits and ensure precise positioning in the designated spots. Compared to other thruster technologies, on-off chemical thrusters can be relatively cost-effective, especially for large-scale satellite constellations. So, more thrust per unit of propellant is obtained for rapid maneuvers or large orbit changes in GEO satellites. Thus, it contributes to their reliability and reduces the risk of failure. So it is important for minimizing fuel consumption and extending the satellite's operational life.

However, their on-off nature can cause small disturbances during maneuvers and the finite amount of propellant limits their lifespan. The thrusters model is used in tandem with MILP and MPC to ensure smooth and efficient satellite maneuvering, which is crucial for maintaining the delicate balance of satellites in geostationary orbits. The accurate model of the discrete nature of on-off chemical thrusters enables realistic simulations and control strategies.

The amount of propellant forced out with an exhaust velocity $\mathbb{V}_e$ from the nozzle of each thruster is expressed as [27]:

$$\mathbb{F} = \mathbb{V}_e \dot{m} + \mathbb{A}_c(\rho_{gas} - \rho_p) = \dot{m} \upsilon_{\text{eff}} \tag{4}$$

Where $\dot{m}$ is the propellant flow rate, A_c is the cross-sectional area of the nozzle exit, and ρ_{gas} and ρ_p are the gas and the ambient pressure, respectively. Parameter υ_{eff} is the effective exhaust velocity of the forced-out mass concerning the satellite. The spacecraft acceleration $\mathbb{a}_s$ is defined as [27,28]:

$$\mathbb{a}_s = \frac{\delta \upsilon}{\delta t} = \frac{\mathbb{F}}{m(\tau)} = \upsilon_{\text{eff}} \left(\frac{\dot{m}}{m(\tau)} \right), \tag{5}$$

The station-keeping maneuver is performed by adding or subtracting delta velocity from the satellite's velocity as [28]:

$$\Delta V = \tau_0^{\tau_0 + \Delta\tau} \mathbb{a}_s d\tau, \tag{6}$$

$$\text{or} \quad \Delta V = -\left(\frac{\mathbb{F}}{m} \right) ln \left(1 - \dot{m} \frac{\Delta\tau}{m_0} \right) \tag{7}$$

After each maneuver, the spacecraft mass $m(\tau)$ decreases during its lifetime due to the consumed propellant [27,29]:

$$m(\tau) = m_0 - \dot{m}\tau \tag{8}$$

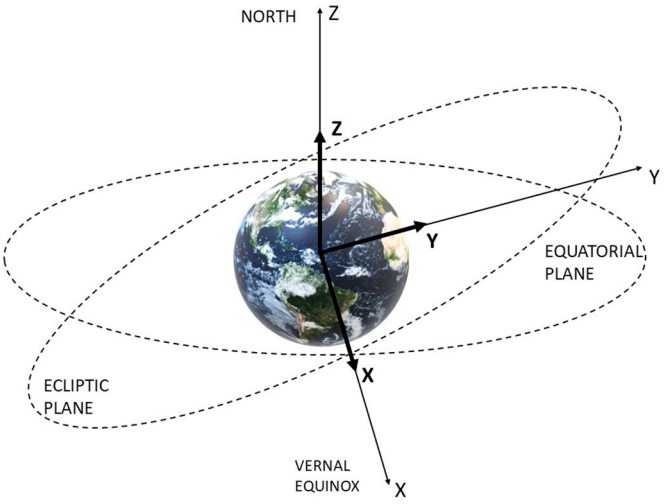

Fig. 4. ECI reference frame offers a stable orientation relative to the celestial sphere and is a reference frame centered at the Earth's core. The positive x-axis aligns with the vernal equinox, while the z-axis aligns towards the celestial north pole. The y-axis is orthogonal to both the x and z axes.

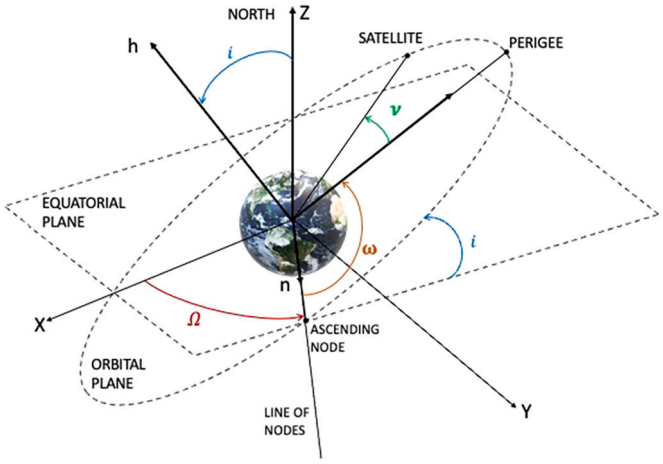

Fig. 5. Equinoctial reference frame: the primary axis E forms an angle equivalent to $-I\Omega$ with the line of nodes. The retrograde component of coefficient I assumes a value of +1 for direct orbits and -1 for retrograde orbits. The W axis is orthogonal to the orbit and aligns with the angular momentum vector, while the Q axis is normal to both E and W axes.

where (m_0) is the spacecraft initial mass and (τ) is the time of the applied maneuver. The thruster specific impulse (I_{sp}) indicates how efficiently the propellant is transformed into proper thrust. The total specific impulse is calculated as [29]:

$$I_{sp} = \frac{\mathbb{F}}{(g\dot{m})} = \frac{v_{eff}}{g} \tag{9}$$

2.4. Coordinate reference frames

For addressing station-keeping, various coordinate reference systems have been proposed to define the satellite parameters, e.g., attitude and velocities. These reference frames are vital for satellite modeling and navigation, i.e., for measuring and predicting the motion of the satellite. In general, each frame has its advantages and limitations depending on the required analysis or application.

2.4.1. International terrestrial reference frame (ITRF)

For instance, a global coordinate system, e.g., ITRF, defines the Earth's center of mass as its origin. The axes align with an established set of defined points on the Earth's surface for the precise determination of satellite positions.

2.4.2. Body reference frame

The sensor measurements and the actuator position are expressed in the body frame, which is fixed relative to the satellite's structure and located at the mass center. The X and Y axes are not aligned with the principal axis.

2.4.3. Earth-centered inertial frame

The Earth-Centered Inertial (ECI) frame enables precise computations of satellite motion, including positions and velocities, from an Earth-centered perspective. This frame, depicted in Fig. 4, explicitly accounts for the time dependency of dynamics, incorporating factors, e.g., geomagnetic field. Situated at the center of the Earth, the ECI frame also represents external torques. The ECI frame serves as a fundamental reference for various applications, e.g., satellite orbit determination, propagation, and tracking [29,30].

2.4.4. Equinoctial reference frame

The equinoctial reference frame is anchored to the celestial equator, maintaining a fixed orientation relative to the stars for delineating the movement of celestial objects relative to Earth. It offers a convenient framework for analyzing orbits characterized by low inclinations, nearly circular eccentricities, and the influence of perturbations on spacecraft trajectories. The equinoctial frame is defined by an orthonormal vectors E, Q, and W, as depicted in Fig. 5. Its stability and well-defined nature make it invaluable for precise calculations and analysis, particularly for circular orbits around Earth [29,31].

After presenting the satellite's dynamics and kinematics, any vector defined in any frame is transformed into another frame using, e.g., direction cosine matrix or quaternion.

2.5. Celestial orbits elements

Practically, the dynamics and trajectory of satellites within space are governed by the characteristics of the celestial orbits. These elements facilitate precise computations of its positional and velocity parameters at any given instance. In the literature, the circular and elliptical orbits are mainly defined by classical orbital elements (COEs) and equinoctial orbital elements (EOEs) [28]. For instance, COEs encounter two primary singularities when defining GEO satellites. The first singularity arises when the orbit is in perfect circularity with zero eccentricity ($\mathbb{e} = 0$), rendering the line of apsides and the argument of perigee undefined. The second singularity occurs when the orbit aligns precisely with the equatorial plane, resulting in zero inclination ($\mathbb{i} = 0$), whereby the ascending node and the right ascension of the ascending node become indeterminate.

On the other hand, the EOEs define the satellite trajectory in nearly circular or near-equatorial orbits. They have many advantages over COEs, e.g., being easier to use, more stable numerically, and resolving the singularities of GEO satellites [31]. For instance, the semi-major axis ($\mathbb{a}$) determines the orbit size. The mean longitude L_m denotes the angular position of the satellite within its orbit, referenced from a specific direction. The orbit eccentricity describes how elongated or circular it is, i.e., the two components of the equinoctial eccentricity, $\mathbb{e}_\tau$ and $\mathbb{e}_n$, signify the orbit eccentricity along the X and Y directions, respectively. Furthermore, the inclination $\mathbb{I}_\tau$ and $\mathbb{I}_n$ within equinoctial elements denotes the orbit tilt relative to a reference plane, e.g., ECI, in the X and Y directions, respectively. These elements facilitate precisely calculating and predicting a satellite movement and describing their orbits accurately [32].

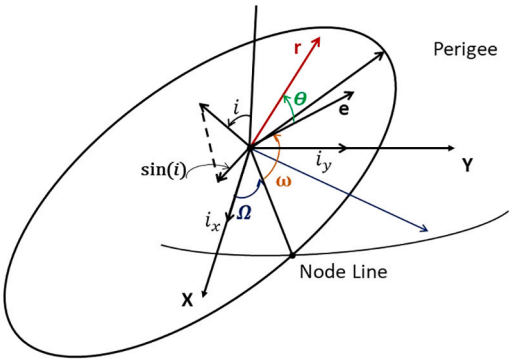

Fig. 6. Geostationary orbital parameters, e.g., semi-major axis a, inclination i, eccentricity e right ascension of the ascending node Ω, argument of perigee ω and true anomaly θ.

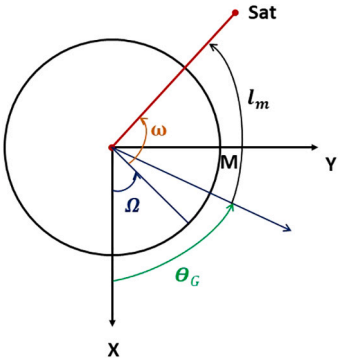

Fig. 7. Equatorial plane orbital parameters along with inertial X, Y coordinate systems, e.g., right ascension of ascending node Ω, argument of perigee ω and mean anomaly M.

2.5.1. EOEs calculation

In this work, the underlying satellite is flying in a nearly equatorial orbit. See Fig. 6 and Fig. 7. So the sidereal angle (α) is expressed in terms of (ω, Ω, θ) [33]:

$$\alpha = \omega + \Omega + \theta, \tag{10}$$

Moreover, instead of the mean anomaly, the mean longitude (L_m) is employed [29].

$$L_m = \omega + \Omega + \theta + M - \theta_G \tag{11}$$

θ_G represents the sidereal angle of the Greenwich meridian, i.e., the angle between the vernal equinox and longitudinal meridian.

The perigee and apogee positions within GEO orbits exhibit considerable uncertainty due to their near-zero eccentricity and inclination. So ω, Ω, and θ are assumed to be nearly coplanar. The norm of the inclination equals the inclination's value (𝕚). Its vector components, $\mathbb{I}_\tau$ and $\mathbb{I}_n$ are proportionate to the right ascension Ω and are aligned respectively along the X and Y inertial axes [33]:

$$\mathbb{I}_\tau = \mathbb{i} cos(\Omega), \tag{12}$$

$$\mathbb{I}_n = \mathbb{i} sin(\Omega). \tag{13}$$

The eccentricity 𝕖 is equivalently expressed as $\mathbb{e}_\tau$ and $\mathbb{e}_n$, which are aligned along the X and Y inertial axes, respectively. It aligns with the radius vector, extending from the center of the attracting body to the perigee, and is contingent on ω and Ω [33]:

$$\mathbb{e}_\tau = \mathbb{e} cos(\Omega + \omega), \tag{14}$$

$$\mathbb{e}_n = \mathbb{e} sin(\Omega + \omega), \tag{15}$$

$$L_m = \mathbb{M} + \omega + \Omega - \theta_G. \tag{16}$$

2.5.2. GEO orbit corrections calculation

The GEO orbit parameters are adjusted by incrementally incorporating $\Delta\mathbb{V}$ components into the satellite velocity within its orbit. As depicted in Fig. 3, the thrusters 6 and 7 add $\Delta\mathbb{V}_r$ along the satellite radius vector. The thrusters 1, 2, and 3 add $\Delta\mathbb{V}_n$ perpendicular to the orbit plane. The thrusters 4 and 5 add $\Delta\mathbb{V}_\tau$ tangential to the velocity vector. The computation of the variation rate in the inclination components along the X and Y axes is determined as follows [24,25].

$$\Delta\mathbb{I}_\tau = \frac{\Delta\mathbb{V}_n}{\mathbb{V}_s} cos(\alpha), \tag{17}$$

$$\Delta\mathbb{I}_n = \frac{\Delta\mathbb{V}_n}{\mathbb{V}_s} sin(\alpha). \tag{18}$$

The rate of change of the eccentricity is defined as [25,29]:

$$\Delta\mathbb{e}_\tau = 2\frac{\Delta\mathbb{V}_\tau}{\mathbb{V}_s} cos(\alpha) + \frac{\Delta\mathbb{V}_r}{\mathbb{V}_s} sin(\alpha) \tag{19}$$

$$\Delta\mathbb{e}_n = 2\frac{\Delta\mathbb{V}_\tau}{\mathbb{V}_s} sin(\alpha) - \frac{\Delta\mathbb{V}_r}{\mathbb{V}_s} cos(\alpha) \tag{20}$$

The rate of change in the mean longitude L_m and the semi-major axis is as follows [24].

$$\Delta L_m = -2\frac{\Delta\mathbb{V}_r}{\mathbb{V}_s}, \tag{21}$$

$$\Delta\mathbb{a} = 2\mathbb{a}\frac{\Delta\mathbb{V}_\tau}{V_s}. \tag{22}$$

Where $\mathbb{V}_s = 3074 m/s$ is GEO satellite velocity.

3. Proposed MILP-MPC methodology

In this work, the proposed controller is designed to achieve various mission requirements, e.g., specified pointing accuracy, while minimizing energy consumption despite perturbations. Moreover, the proposed controller has to consider the orbital dynamics and the satellite constraints, e.g., actuator limitations. To achieve these requirements, we propose a MILP-MPC for the GEO satellite, see Fig. 8. MILP-MPC solves a finite-horizon optimization problem optimizing performance objectives, e.g., station-keeping and energy consumption, i.e., firing time.

3.1. MILP-MPC potentials for station-keeping

The proposed MILP-MPC achieves significant advantages and features over other traditional methods, especially for satellite station-keeping.

- Predictive Nature using satellite dynamics anticipates future behavior to determine the control actions for achieving desired missions.
- Systematic handling of space mission limitations and satellite constraints, e.g., communication link requirements, collision avoidance, thrust firing, and fuel consumption limits.
- Considering the satellite kinematics and orbital dynamics to ensure the solution feasibility.
- Optimal performance, e.g., precise station-keeping and fuel-efficient maneuvers, i.e., energy consumption and firing time.
- Inherent robustness for model uncertainty and perturbations, e.g., gravity-gradient torque.
- Fault tolerance capabilities, e.g., thruster failure.
- Integer decision variables for switching on/off various thrusters in different maneuvers.
- Incorporating different durations for each thruster.
- Incorporating different weights for various maneuvers, e.g., east/west or south/north.
- Real-Time Adaptation to changing conditions, e.g., unexpected disturbances or new constraints, by replanning the control actions at each time step.

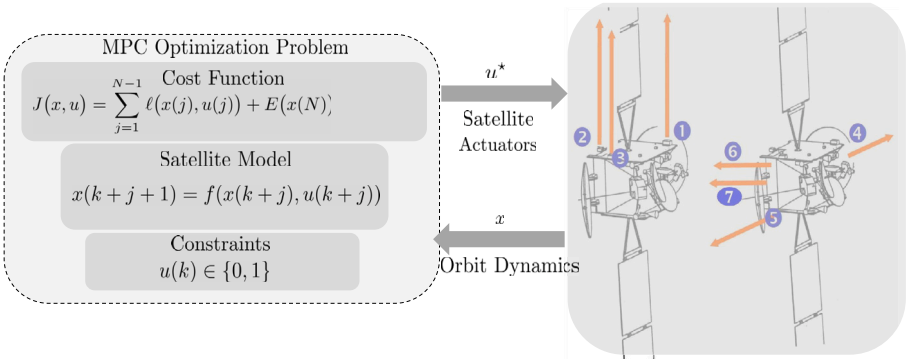

Fig. 8. Block diagram of MILP-MPC station-keeping system: at each time step, the satellite orbital dynamics is predicted over a finite prediction horizon. Optimal control input is calculated based on the repeated solution of the optimal control problem satisfying system constraints and optimizing a cost function.

- Integration with other satellite subsystems, e.g., attitude control and communication systems, to provide a coordinated and optimized approach to overall satellite operation.

With these remarkable potentials, the MILP-MPC in satellite attitude control has the potential to revolutionize space missions. MILP-MPC improves the satellite stability, accuracy, and overall operational efficiency while ensuring precise positioning and orientation of satellites. In GEO station-keeping, MPC offers a proactive approach by anticipating the satellite trajectory and planning maneuvers to counteract perturbations, ensuring precise orbital positioning. Moreover, MPC allows satellite operators to proactively assess potential collision threats and make informed decisions to ensure the continued operation and safety of GEO satellites.

MILP helps optimize satellite trajectories by considering discrete variables, while MPC looks ahead, predicting the future movement of satellites to make smart decisions in real-time.

3.2. MILP-MPC scheme

This section outlines the basic scheme of the MILP-MPC mathematical formulation, including the objective function, sampling time, prediction horizon, satellite model, and constraints. At each time step t_k, MILP-MPC leverages a mathematical model and current state x_0 to predict the satellite kinematics and orbital dynamics over a *prediction horizon* $T = N \cdot T_s$ to determine the optimal control sequence

$$\mathbb{u}^\star = \{u(t_k), u(t_{k+1}), \dots, u(t_{k+N_c})\} \in \mathbb{R}^{(N.n_u)}.$$

The determined solution online optimizes the station-keeping performance and energy consumption. At the current step, only the first element $u(t_k)$ of the obtained control sequence $\mathbb{u}^\star$ is applied to the satellite actuators to modify the satellite attitude until the next sample t_{k+1}. Then, the predictions and optimization are repeated periodically using the new measurements, see Fig. 8 [34,35]. MILP-MPC can handle the deviation between the satellite's predicted and actual response due to, e.g., model inaccuracy or unmeasured perturbations. Practically, it is necessary to specify a suitable *sampling time* $T_s = t_{k+1} - t_k$ and prediction horizon to achieve the performance requirements, e.g., minimum station-keeping error and to handle high-frequency perturbations while decreasing the computation time.

In this context, MPC allows satellites to be guided on the right path and avoid potential obstacles by analyzing their current state, predicting future behavior, and optimizing control inputs.

In general, understanding these constituents and formulations is crucial in effectively implementing a MILP-MPC to achieve the station-keeping mission while adhering to operational constraints.

3.3. MILP-MPC optimization formulation

Formulating the station-keeping problem as a MILP-MPC can efficiently plan and execute complex maneuvers with precision. This mathematical approach optimizes fuel consumption, trajectory planning, and overall mission success.

The mathematical formulation of the proposed MILP-MPC for station-keeping is represented as

$$\min_{x,u} J = \min_{x,u} \sum_{j=1}^{N-1} \ell(x(k+j|k), u(k+j|k)) + E\big(x(k+N|k)\big), \tag{23a}$$

$$\text{s.t.} \quad \forall j \in \{0, ..., N-1\}$$

$$x(k|k) = \hat{x}(k), \tag{23b}$$

$$x(k+j+1|k) = f\big(x(k+j|k), u(k+j|k)\big), \tag{23c}$$

$$x(k+j|k) \in \mathbb{X}, \quad u(k+j|k) \in \mathbb{U}, \tag{23d}$$

$$x(k+N|k) \in \mathbb{X}_T. \tag{23e}$$

Here, $x \in \mathbb{R}^{n_x}$ are the satellite states, e.g., six equinoctial orbital parameters ($\mathbb{a}$, $\mathbb{I}_\tau$, $\mathbb{I}_n$, $\mathbb{e}_\tau$, $\mathbb{e}_n$, and $\mathbb{L}_m$). The argument $(k+j|k)$ denotes the j-th future prediction of the satellite state made at the time step k. $x(k|k)$ and $\hat{x}$ are the initial condition and estimated value of the satellite state. Eq. (23d) are the satellite constraints.

3.3.1. System model and prediction

The proposed strategy uses a satellite model to predict its future behavior to determine optimal control decisions. This model should accurately predict satellite performance while reducing the computational complexity of the controller. Moreover, this model should capture orbital dynamics, propellant consumption, and external perturbations.

$$\forall j \in \{0, ..., N-1\}$$

$$x(k+j+1|k) = f(x(k+j|k), u(k+j|k)), \tag{24}$$

where $x \in \mathbb{R}^{n_x}, u \in \mathbb{R}^{n_u}$ are the controlled state and the manipulated inputs with dimensions n_x, n_u respectively. The proposed MILP-MPC predicts the satellite performance using an appropriate model $f : \mathbb{R}^{n_x} \times \mathbb{R}^{n_u} \to \mathbb{R}^{n_x}$ starting from an initial measured state x_0 to determine input u. Combining MILP-MPC with satellite dynamics models leads to an increase in the precision and efficiency of the station-keeping algorithm.

3.3.2. State and input constraints

To ensure safe operations, the proposed MILP-MPC explicitly considers a wide range of satellite constraints, such as fuel consumption limits, maneuver planning requirements, collision avoidance, and communication link constraints. These constraints represent the operation

boundaries and the state limitations, e.g., maximum velocity and accelerations, and input restrictions:

$$\forall j \in \{0, ..., N-1\}$$

$$x(k+j|k) \in \mathbb{X}(k+j|k) \subset \mathbb{R}^{n_x}, \tag{25a}$$

$$u(k+j|k) \in \mathbb{U}(k+j|k) \subset \mathbb{R}^{n_u}. \tag{25b}$$

The state $\mathbb{X}$ and input $\mathbb{U}$ constraints sets. Moreover, extra constraints might be added to achieve stability and recursive feasibility of the proposed optimization problem. For instance, the obtained solution, i.e., state, must fulfill the terminal constraints at the horizon end, e.g., $x(N) \in \mathbb{X}_T \subset \mathbb{R}^n$ [35]. In this context, these constraints might include fuel limitations, orbital position accuracy requirements, and thrust time limitations. This enables the optimization of satellite maneuvers while ensuring safe and efficient operation.

3.3.3. Receding-horizon scheme

The proposed MPC framework utilizes a receding horizon control strategy to determine the optimal control actions by solving the MILP optimization problem at each time step. This approach allows for real-time adaptation to changing conditions, such as unexpected disturbances or new collision threats. In this work, the optimization problem (23) is solved online at every time k recursively to determine the optimal control sequence $\mathbb{u}^\star(k) = \{u^*(k), u^*(k+1), u^*(k+2), ...u^*(k+N)\}$. Only the first term $u^*(k)$ is sent to the thruster to modify the satellite attitude. At the next time $k+1$, both prediction and optimization are repeated when new measurements are available with a receding horizon fashion. This iterative nature allows for adaptability to changing dynamics and perturbations while always searching for optimal solutions within given constraints. In the same context, MPC continually updates its predictions and control actions based on real-time system measurements, allowing for adaptive and precise control in complex systems.

3.3.4. Integer programming

MILP can handle discrete control inputs, such as on-off thrusters, commonly used in satellite propulsion systems. This allows for more realistic modeling and optimization of control strategies. Formulating the station-keeping and collision avoidance problem as a MILP can effectively handle the discrete nature of thruster actuation and incorporate various constraints, e.g., fuel consumption limits, maneuver planning requirements, and collision avoidance rules. The proposed MILP optimizes the satellite behavior by finding the best inclusion of discrete decision variables for solving complex problems with integer and continuous variables. For instance, $u \in \{0, 1\}$ are binary control inputs, e.g., thruster firing, see Fig. 3. The combination of MILP and MPC offers a potential solution to enhance the decision-making process in satellite control, ensuring the precision of both station-keeping and collision avoidance maneuvers. For instance, MILP helps derive solutions that align with practical satellite operations by incorporating integer variables to represent discrete choices, such as thruster firing patterns and sequencing of maneuvers, MILP allows for the inclusion of discrete decision variables, such as the choice of maneuvers or the timing of maneuvers. This is crucial for collision avoidance, as certain maneuvers might be more effective or less risky than others in preventing collisions.

3.3.5. Objective function

The proposed MILP-MPC can simultaneously optimize multiple objectives, such as minimizing fuel consumption, maneuver error, and communication link disruptions. This provides flexibility in designing control strategies that balance different priorities. The main objective of this work is to execute maneuvering actions to achieve precise orbital positioning and ensure long-term station-keeping performance. At the same time, the objective function incorporates control effort terms to balance accuracy and resource consumption. Thus, MILP-MPC determines an optimal solution minimizing a certain finite horizon cost functional

$$J\left(x,u\right) = \sum_{j=1}^{N-1} \ell\left(x(j), u(j)\right) + E\left(x(N)\right). \tag{26}$$

Herein *stage cost function* $\ell\left(x(\cdot), u(\cdot)\right) : \mathbb{R}^{n_x} \times \mathbb{R}^{n_u} \to \mathbb{R}_0^+$ optimizes the satellite performance, e.g., station-keeping error and energy consumption, over the prediction horizon.

The proposed methodology aims to minimize the cost functional $\ell : \mathbb{R}^{n_m} \times \mathbb{R}^{n_l} \times \mathbb{R}^{n_u} \to \mathbb{R}_0^+$, e.g., satellite trajectories by simultaneously considering mission objectives, fuel efficiency, and collision avoidance criteria.

Terminal cost function $E(x(\cdot)) : \mathbb{R}^{n_x} \to \mathbb{R}_0^+$ represents the cost-to-go of only the satellite state beyond the horizon. The terminal constraint (23e) and cost $E : \mathbb{R}_x^n \to \mathbb{R}_0^+$ are imposed to ensure the controller stability and the solution feasibility. In this work, the weight parameters in the cost function $J(\cdot)$ are tuned properly to balance the satellite performance and the energy consumption simultaneously.

4. Simulation setup and validation

This section presents the simulation setup of the satellite orbital parameters and the corresponding numerical outcomes achieved after performing the planned station-keeping and collision avoidance maneuvers. In this work, we use YALMIP [36] to formulate the station-keeping problems, using Gurobi [37] for solving efficiently the optimization problems of the proposed MILP-MPC.

The simulations focus on an existing satellite platform weighing 3476 [kg] and equipped with seven chemical thrusters, each capable of delivering a maximum force thrust ($\mathbb{F} = 10$) [N]. Whereas we set the earth gravitational $g = 9.80665[m/s^2]$, the thruster-specific impulse ($I_{\mathbb{sp}} = 300$) [s], the mass flow rate ($\dot{m} = 3.5$) [g/s], and the ejection velocity $v_{eff} = 3500$ [m/s]. It is important to highlight that the same satellite platform used to implement and validate both the RCT model in [24] and the orbit determination model in [25] is also utilized in this study. The satellite's total mass varies dynamically during station-keeping maneuvers and is recalculated before each new maneuver is initiated.

The output of the proposed MILP-MPC model includes six equinoctial orbital parameters ($\mathbb{a}$, $\mathbb{l}_\tau$, $\mathbb{l}_n$, $\mathbb{e}_\tau$, $\mathbb{e}_n$, and $\mathbb{L}_m$). The efficacy of the proposed MILP-MPC control model is evaluated by simulating ten consecutive cycles of planned station-keeping maneuvers, each comprising south-and-east maneuvers, and comparing the total time required to perform each cycle of the maneuvers with an existing active satellite platform (Eurostar-3000) that is used in [24,25].

4.1. Planned station-keeping maneuver

The purpose of the planned station-keeping maneuvers on GEO satellites is to maintain their designated orbital positions relative to the Earth's surface. By periodically adjusting the satellite orbit by planning station-keeping maneuvers every 14 days to counteract the effects of external perturbations, thereby preventing drift and ensuring that they remain stationary relative to a fixed point on Earth's surface.

First, the south maneuver and then the east maneuver is performed. On the other hand, the precise orbit of the satellite calculated on the ground is uploaded to the satellite before the next maneuver, which is planned after 14 days to repeat the maneuver cycle every two weeks.

4.1.1. South maneuver

The south maneuver is done three to four days before the east maneuver. Thus, the errors that may arise from the south maneuver are prevented from growing exponentially. The east maneuver is a corrective maneuver that includes these effects. GEO satellites are ideally located within a window, typically $\pm 0.1^\circ$ from the equatorial plane, as shown in Fig. 1.

The south maneuver is performed at ascending or descending nodes to adjust the angle between the orbit and ecliptic planes. As illustrated

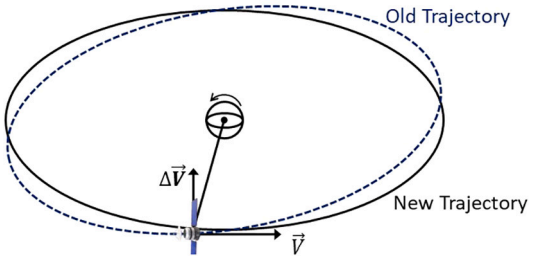

Fig. 9. South maneuver adjusts the angle between the orbit and ecliptic planes.

in Fig. 9, this maneuver involves applying a $\Delta\mathbb{V}$ perpendicular to the orbital plane, denoted as $\Delta\mathbb{V}_n$ in the Y direction normal to the orbit, at the elevation point. The effect of $\Delta\mathbb{V}_n$ on the old and new trajectories is depicted in Fig. 9, emphasizing its role in correcting the orbit inclination, which is essential for calculating the variations in the inclination components ($\mathbb{I}_\tau, \mathbb{I}_n$) resulting from the firing of thrusters 1, 2, and 3, as outlined in Eq. (17).

Fig. 10 and Fig. 11 illustrate the final inclination in the X and Y directions, respectively, after performing the south maneuver, which corrects the deviation in orbit inclination caused by geophysical perturbation factors. The figures show that the final inclination values are close to zero, indicating that the satellite's orbit is nearly parallel to the equator. This alignment is crucial for maintaining the satellite's position within the station-keeping box, ensuring consistent communication between the satellite and the designated ground control center.

Fig. 10 and Fig. 11 depict the outcomes of the proposed system compared with the real system, illustrating the transition of the satellite's initial values to the reference values after the successful execution of the maneuver. The figures demonstrate the convergence of the inclination components ($\mathbb{I}_\tau$ and $\mathbb{I}_n$), respectively, from their initial state to the desired reference values after the total firing time of all thrusters.

4.1.2. East maneuver

In the east maneuver, the delta velocity $\Delta\mathbb{V}$ is added to the satellite moving along the drift with the linear velocity $\mathbb{V}$ denoted as $\Delta\mathbb{V}_\tau$ in the X direction tangential to the orbit which is essential for calculating the variations in the eccentricity components ($\mathbb{e}_\tau, \mathbb{e}_n$) and the semi-major axis ($\mathbb{a}$) resulting from the firing of thruster 4, as outlined in Eqs (19), (20), (22). In this case, the satellite accelerates and moves into a higher orbit, thus shifting west relative to the Earth. Fig. 12 shows the GEO satellite orbit before and after the east maneuver. After performing the maneuver, the orbital period is controlled, and the satellite is in the

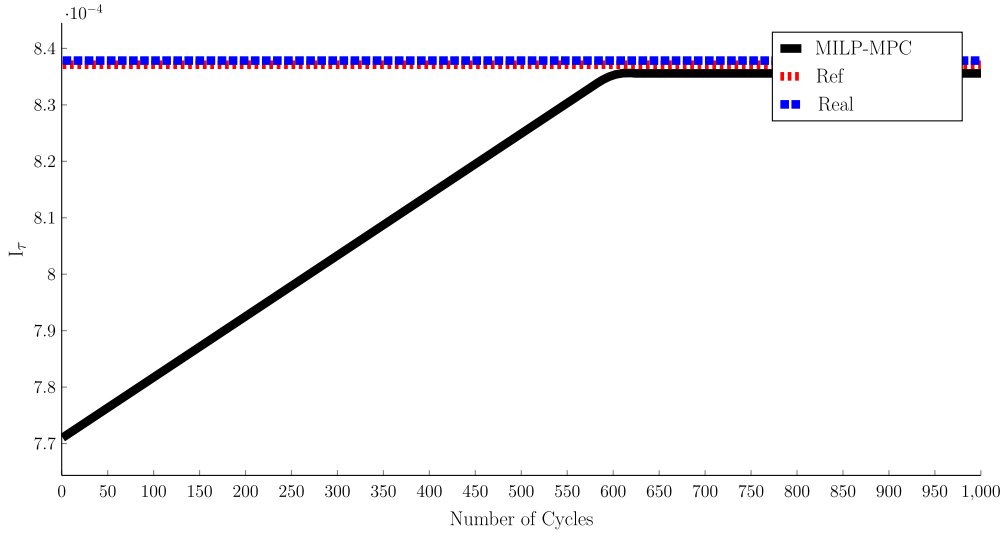

Fig. 10. The convergence of the inclination ($\mathbb{I}_\tau$) from its initial state to the desired reference value is compared with that of the real system after the south maneuver.

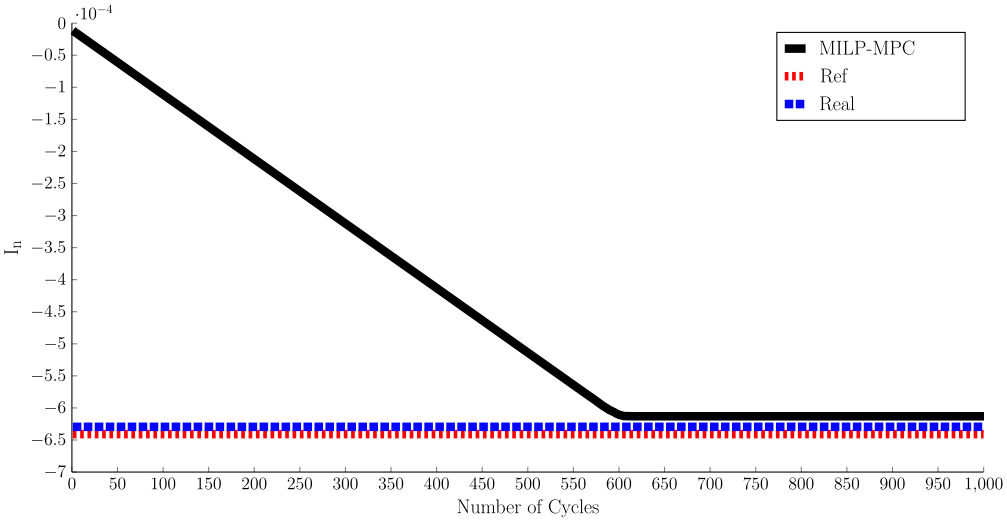

Fig. 11. The convergence of the inclination ($\mathbb{I}_n$) from its initial state to the desired reference value is compared with that of the real system after the south maneuver.

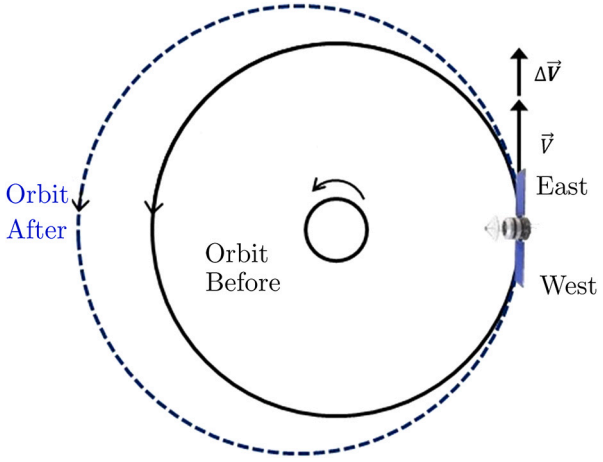

Fig. 12. East maneuver accelerates the satellite and moves it into a higher orbit.

predefined longitude. Fig. 13 and Fig. 14 demonstrate the successful convergence of the satellite's orbital parameters, including eccentricity and semi-major axis, from their initial states to the desired reference values after the completion of all thruster firings.

Fig. 13 and Fig. 14 demonstrate the resultant values of the semi-major axis and eccentricity of the satellite orbit after performing the east maneuver. This maneuver corrects the deviation in the satellite's eccentricity caused by geophysical perturbation factors, returning it to a value nearly equal to zero. Maintaining this near-zero eccentricity is essential for preserving the circularity of the GEO satellite's orbit, ensuring that the satellite remains within its designated station-keeping box and maintaining a stable communication link between the satellite and the ground control center.

Table 1 and Table 2 depict the numerical values of the satellite EOEs. The initial values denote the satellite state before executing the maneuver, while the reference values represent the desired parameters after the maneuver. The MILP-MPC output corresponds to the proposed system values post-maneuver application and the real-time telemetry data from the existing satellite platform. The simulation outcomes assess the efficacy of the proposed MILP-MPC controller, facilitating a comparison between the model results and those obtained from existing spacecraft data.

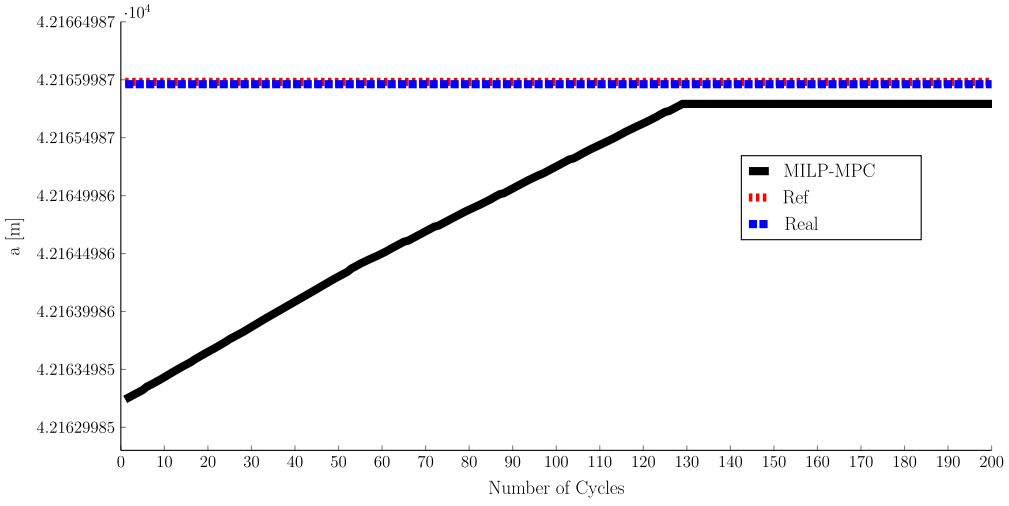

Fig. 13. The evaluation of the alignment of the semi-major axis (a) from its initial state to the desired reference value is performed by comparing it with the real system after the east maneuver.

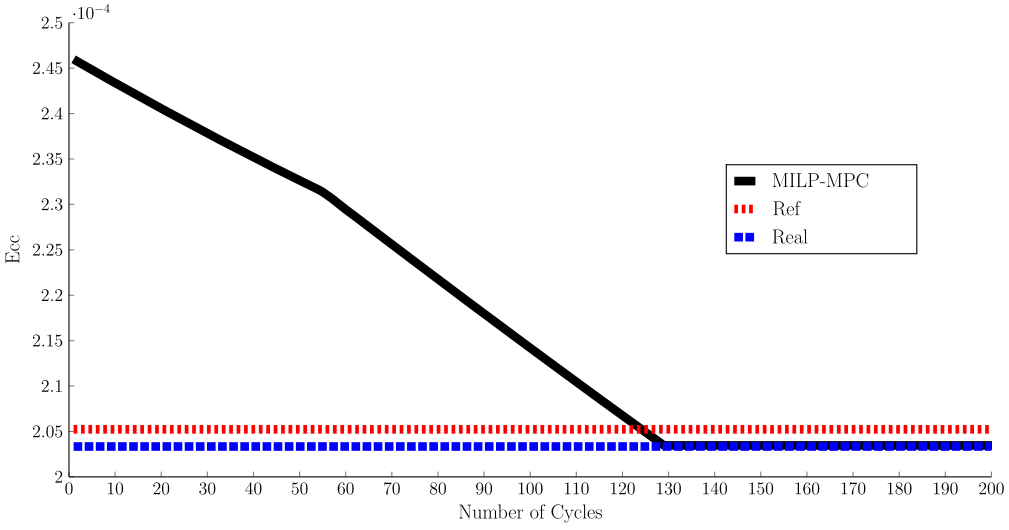

Fig. 14. The alignment of the eccentricity (e) from its initial state to the desired reference value is evaluated in comparison with the real system after the east maneuver.

The proposed model effectively achieves the desired orbit through ten successive maneuver cycles, encompassing both south and east maneuvers, starting from various initial states. Simulation results confirm the efficacy of the approach, validated through comparison with real data extracted from an existing satellite platform (Eurostar-3000). Specifically, the results presented in Table 1, Fig. 10, and Fig. 11 for the south maneuver, and Table 2, Fig. 13, and Fig. 14 for the east maneuver.

Practically, each thruster is specified with a different activation duration at each cycle for the south and east maneuvers. The control signals $\{u_1, \ldots, u_7\}$ to activate the seven thrusters delineate the duration of activation required for each thruster during the south and east maneuvers, as depicted in Fig. 15 and Fig. 16, respectively. Each thruster is activated once within each sample interval, set at 1.4 [s]. The resulting duty cycles vary for each thruster based on the maneuver type and the number of thrusters involved, as illustrated in Fig. 17 and Fig. 18, respectively.

Fig. 15 and Fig. 16 depict the accumulation of control signals, denoted by u_1 to u_7, used to activate the respective on-time duration of the seven thrusters. Each control signal corresponds to a specific thruster and contributes to the total number of firing time pulses for that thruster. These cumulative pulses are then utilized to calculate the total firing time of each thruster. Fig. 17 and Fig. 18 illustrate the process of activating the thrusters firing time. Each thruster is activated only once within each sample interval, with no consecutive activation pulses occurring within the same sample. The next activation time occurs after the 1.4-second interval in the subsequent sample, depending on the specific control signal sent to activate the thruster's firing time.

The proposed method allows for keeping the satellite in the desired attitude configuration and maintaining it in the station-keeping box, as depicted in Fig. 1.

4.2. Collision avoidance maneuver strategy

The huge number of satellites orbiting Earth increases the collision risk. The MPC system can continuously monitor the satellite trajectory and other satellites in the vicinity and adjust the planned maneuvers to avoid potential collisions. MILP can be used to optimize the choice of maneuvers and the timing of maneuvers to minimize the risk of collisions while achieving the desired mission objectives. So, satellite operators must constantly monitor potential collision threats and maneuver satellites out of harm's way to ensure the continued operation and safety of GEO satellites. For instance, the satellite control center assesses potential collision risk by analyzing the predicted paths of space debris relative to the satellite's orbit. It considers the debris's size, velocity, and trajectory from the Collision Data Message (CDM). Then, develop collision avoidance maneuver plans by calculating the required changes in delta-velocity ($\Delta\mathbb{V}$) to alter the satellite's trajectory and avoid the predicted collision. When planning the maneuver, consider various operational constraints, such as fuel availability, thruster capabilities, orbital stability, and mission objectives. The first scenario plans an east maneuver to enlarge the orbit until the space debris passes, as depicted in Fig. 19.

Then, the West maneuver is executed to return to the orbit as presented in Fig. 20.

The second scenario begins with the West maneuver to reduce the orbit and return it by performing the East maneuver after the space debris passes. The best scenario is chosen depending on the position of the space debris to get a safe distance between the space debris and the satellite, as shown in Fig. 21.

To validate the proposed MILP-MPC method and demonstrate its efficiency, we present a real case involving a collision avoidance maneuver between an existing satellite and space debris. This validation is based on the analysis of a CDM received from the Joint Space Operations Center (JSpOC) on May 30, 2022. JSpOC conducts space surveillance to monitor satellites, space debris, and other space assets, thereby maintaining situational awareness and identifying potential collision risks. The CDM plays a crucial role in managing collision risks by providing comprehensive information about potential threats and recommended response actions, enabling satellite operators to take proactive measures to ensure mission safety. The CDM includes details of a close

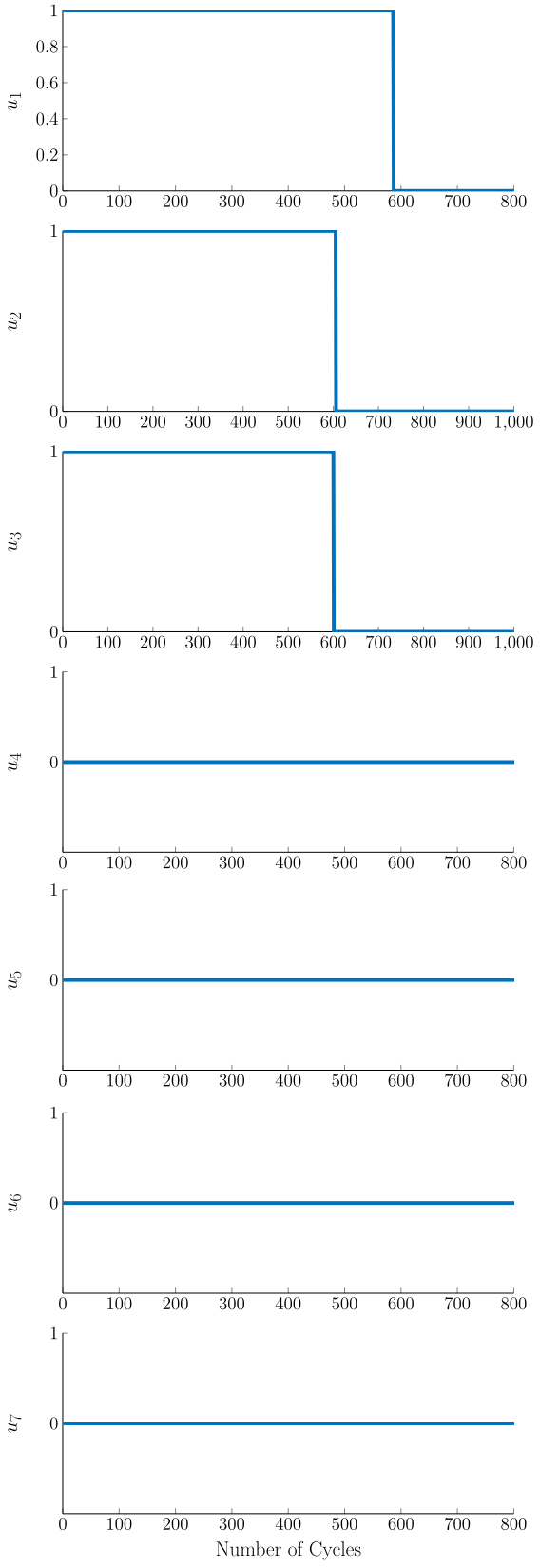

Fig. 15. On/OFF thrusters in the south maneuver.

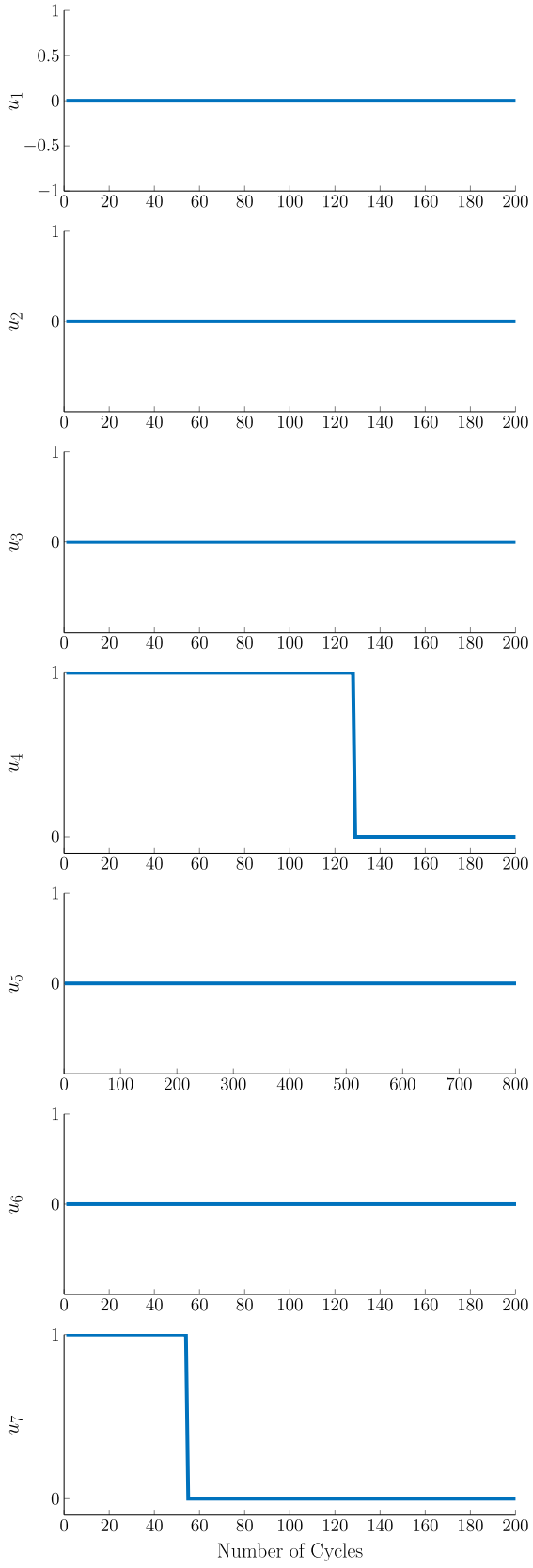

Fig. 16. On/Off thrusters in the east maneuver.

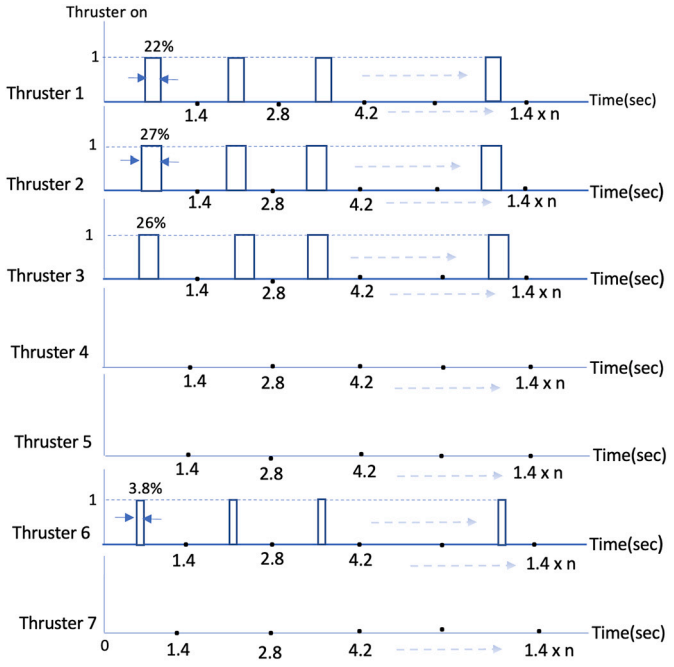

Fig. 17. Thruster On/Off time of the south maneuver.

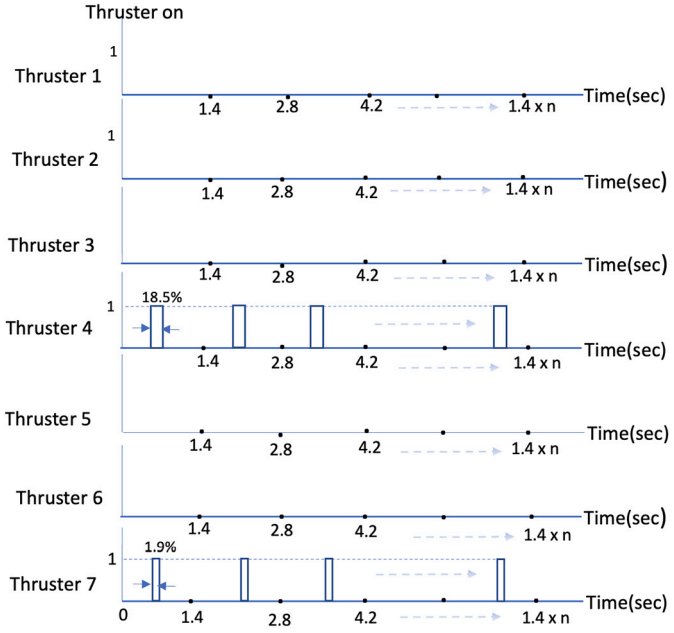

Fig. 18. Thruster On/Off time of the east maneuver.

approach between the existing satellite and space debris scheduled for 02/06/2022, with a close approach time of 05:51:09 UTC. The miss distance is 9.47 km, with relative radial, tangential, and normal positions of 2.49 km, 9.06 km, and 1.2 km, respectively. Based on the CDM, the observed radial separation is 2.49 km less than the minimum safe distance, as the minimum safe radial separation is 5 km, indicating a potential collision risk. To mitigate this risk, a collision avoidance maneuver will be performed. The maneuver will commence with a west maneuver to reduce the orbit, as the radial position of the debris is positive. Once the close approach of the debris concludes and it safely passes, an east maneuver will be executed to return the orbit to its original state.

This strategy ensures the safety and integrity of the satellite mission by proactively avoiding the possibility of collision with the debris. This analysis provides empirical data to evaluate the performance of the MILP-MPC method in managing collision avoidance scenarios, showcasing its ability to mitigate collision risks and maintain satellite mission

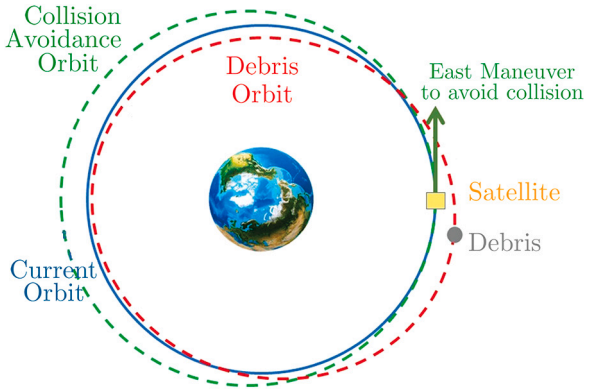

Fig. 19. Collision avoidance east maneuver expands the orbit during space debris passage.

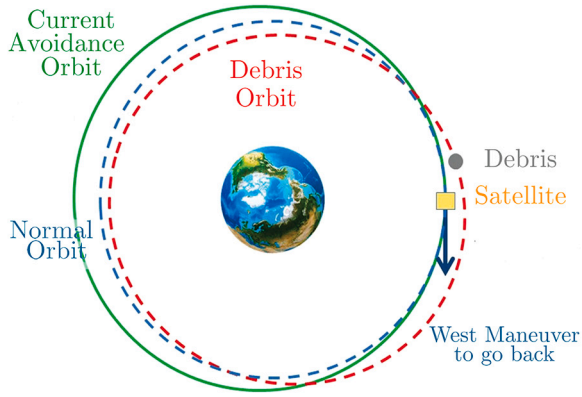

Fig. 20. Collision Avoidance west maneuver returns the orbit to its initial state.

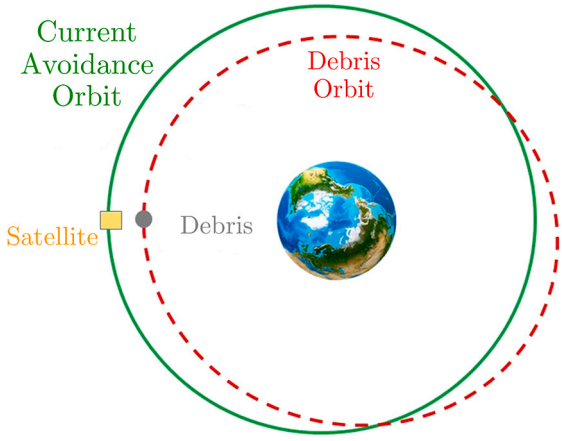

Fig. 21. Satellite orbit after collision avoidance maneuver.

integrity effectively with minimum fuel consumption and the same performance. Specifically, the results presented in Table 3, Fig. 22, and Fig. 23 for the collision avoidance maneuver. The proposed method allows for avoiding the passes of space debris and maintaining the satellite in the station-keeping box.

Fig. 22 shows the effect of the west maneuver on the semi-major axis, which reduces its value to shrink the orbit by a specified amount, allowing the satellite to avoid debris during its passage safely. Fig. 23 illustrates the effect of the east maneuver, which enlarges the orbit by increasing the semi-major axis value to restore the satellite's orbit to its defined position. During both the collision avoidance west and east maneuvers, the satellite remains within the station-keeping box, ensuring uninterrupted communication between the satellite and the ground control center.

Fig. 22 and Fig. 23 demonstrate the successful convergence of the satellite semi-major axis, from its initial states to the desired reference value after the completion of all thruster firings. Table 3 depicts the numerical values of the satellite EOEs. The "initial values" denote the satellite's state before executing the maneuver, while the "reference values" represent the desired parameters after the maneuver.

The MILP-MPC performance corresponds to the proposed system values post-maneuver application, and the real system values are the extracted data from the existing satellite platform. The simulation outcomes assess the efficacy of the proposed MILP-MPC controller model, facilitating a comparison between the model results and those obtained from the real-case collision avoidance maneuver. To ensure successful collision avoidance, the satellite's trajectory and the evolving positions of nearby space debris should be continuously monitored during and after the maneuver. Analyze the effectiveness of the collision avoidance maneuver by evaluating the satellite's new orbit, fuel consumption, and any deviations from the original mission objectives.

4.3. Results discussion

Extensive simulations were conducted to evaluate the performance of the proposed MPC framework under various scenarios, demonstrating its effectiveness in achieving accurate station-keeping and collision avoidance. Optimization techniques should be employed to find the most efficient maneuver strategy that satisfies the operational constraints and minimizes fuel consumption. After successfully implementing station-keeping and collision avoidance maneuvers using the MILP-MPC controller, simulation results over ten successive cycles (including both south and east maneuvers) and real-world collision avoidance scenarios show a strong correlation with the actual performance of the existing Eurostar-3000 satellite platform, which is designed and manufactured by Airbus Defence and Space. It is widely utilized by satellite operators worldwide for delivering commercial GEO satellite services. Table 1 illustrates the strong correlation between the inclination values in the X and Y directions of the desired reference, actual, and proposed models. This alignment ensures the satellite remains in its desired orbital location while optimizing fuel consumption during the south maneuver.

Table 2 demonstrates the successful alignment of the eccentricity in both the X and Y directions, as well as the semi-major axis, between the proposed system, the desired reference, and the actual values after performing the east maneuver. This consistency highlights the effectiveness of the proposed system in achieving the target orbital parameters.

Table 3 highlights the strong similarity in eccentricity along the X and Y directions and the semi-major axis between the proposed system and the actual and reference values during the collision avoidance west and east maneuvers. This close alignment underscores the effectiveness of the proposed system in accurately replicating the desired orbital adjustments.

The Root Mean Square Error (RMSE) was utilized as a standard metric to measure the difference between the proposed and actual values in regression analysis. The RMSE between the reference values and the real system yielded 1.49×10^{-5} for the inclination during the south maneuver and 1.48×10^{-6} for the eccentricity during the east maneuver. Similarly, the RMSE between the reference values and the proposed system was found to be 1.64×10^{-5} for the inclination in the south maneuver and 5.42×10^{-6} for the eccentricity in the east maneuver. These results, shown in Table 4, demonstrate a close match between the values generated by the proposed model and those from the established Eurostar-3000 satellite platform, showing strong alignment and high precision, with the observed differences remaining within the orbit determination accuracy limits specified in [25].

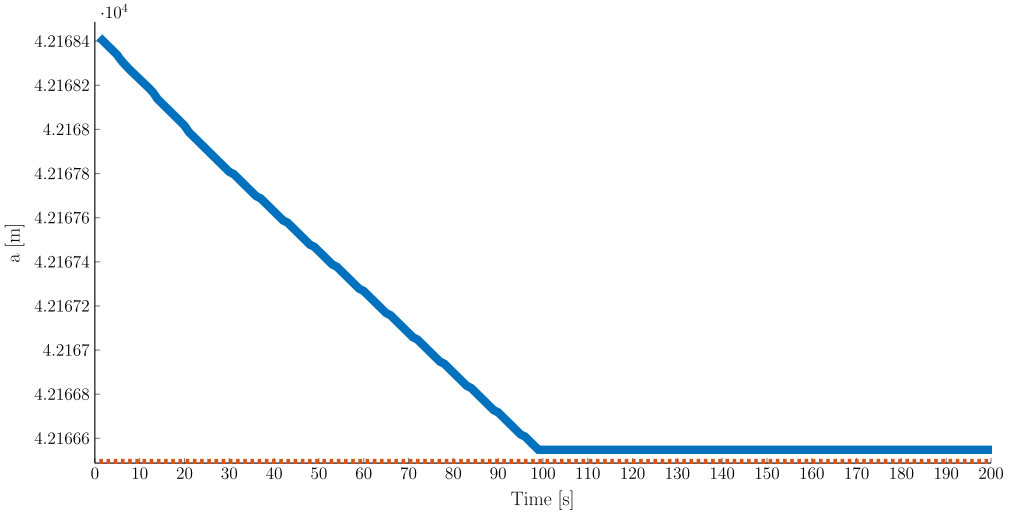

Fig. 22. The convergence of the satellite semi-major axis, from its initial states to the desired reference value after the collision avoidance west maneuver.

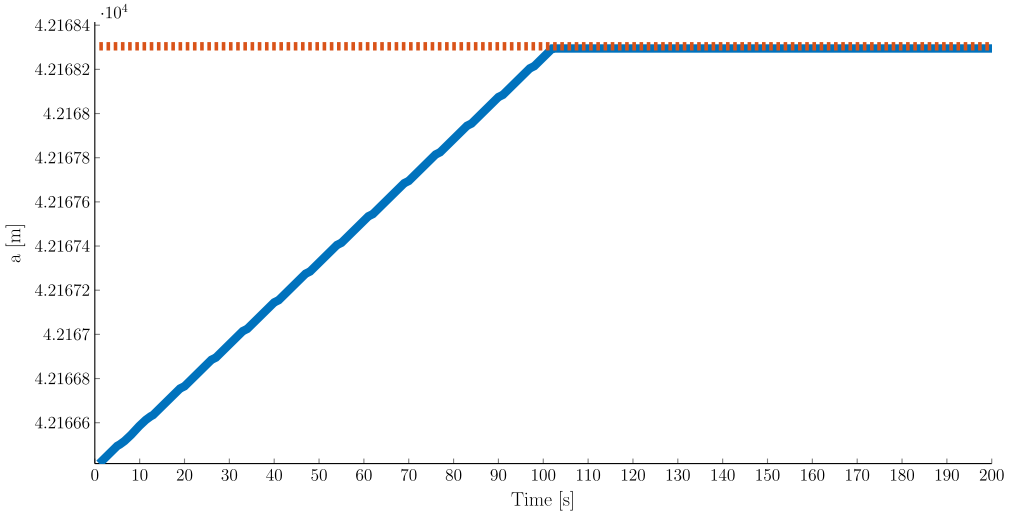

Fig. 23. The convergence of the satellite semi-major axis, from its initial states to the desired reference value after the collision avoidance east maneuver.

The proposed model significantly improves fuel efficiency by optimizing thruster firing times during station-keeping and collision avoidance maneuvers. The results highlight the following key reductions in thruster firing time.

- The total thruster firing time for executing ten consecutive real station-keeping maneuvers is recorded at 6982.489 seconds. The proposed model achieves the same maneuvers with a total firing time of 6403.061 seconds. This represents a reduction of approximately 570 seconds, directly contributing to reduced fuel consumption, as shown in Table 5.
- The total firing time for real collision avoidance maneuvers is recorded at 45.179 seconds. The proposed model reduces this to 38.9256 seconds. This decrease of approximately 6 seconds helps minimize fuel consumption, as detailed in Table 6.

The satellite's operational lifetime spans 15 years, or approximately 780 weeks, requiring about 390 maneuver cycles to maintain its orbital slot. The reduction in firing time through the proposed system contributes significantly to extending the satellite's operational life by reducing fuel consumption. The impact on the satellite's operational lifetime is detailed as follows:

- The average firing time for one station-keeping maneuver cycle (South and East) typically ranges from 700 to 800 seconds, as indicated in Table 5.
- Implementing the proposed system saves 570 seconds for every ten cycles. Over 390 cycles, this results in an estimated total saving of 22,230 seconds.
- This time saving could extend the satellite's operational life by approximately 29 additional maneuver cycles, translating to 58 extra weeks, due to minimized fuel consumption.

The simulation results from the MILP-MPC controller confirm the proposed approach's effectiveness. The model closely aligns with real-world data, demonstrating high accuracy and requiring less total thruster firing time. This confirms the system's efficiency in both station-keeping and collision-avoidance maneuvers.

5. Conclusion and future work

This work proposes an advanced satellite control system for enhanced operational efficiency and safety in space. Combining MILP and MPC strategies offers a powerful framework for optimizing satellite trajectories and fuel consumption for GEO satellite mission objectives, e.g., station-keeping. In this work, we have discussed how the MPC approach

tackles the limitations of traditional methods and showcases its operational efficiency, e.g., station-keeping accuracy and fuel consumption. The proposed approach effectively addresses the challenges associated with planned maneuvers, fuel constraints, and the discrete nature of on-off chemical thrusters.

The proposed MPC has been successfully implemented in different scenarios, e.g., south and east maneuvers and collision avoidance. Incorporating collision avoidance strategies in the proposed MILP-MPC framework effectively mitigates collision risks. The results obtained from performance evaluation and comparative analysis demonstrate the superiority of the MILP-MPC framework in achieving accurate station-keeping and collision-free maneuvers while optimizing fuel consumption. For instance, the proposed approach is a systematic and flexible way to incorporate complex constraints and optimize the control inputs for improving the satellite accuracy, making it well-suited for the dynamic environment of GEO satellite station-keeping. The MILP incorporates integer variables to represent discrete choices, e.g., thruster firing patterns and sequencing of maneuvers. Therefore, MILP leads to derived solutions that align with practical satellite operations and more efficient fuel consumption and trajectory planning. For instance, the proposed controller reduces the total firing time by 555.523 and 23.894 seconds in the south and east maneuvers, respectively, for ten successive maneuver cycles. This reduction increases the satellite's lifetime by 7.5%. MPC promises to reduce operational costs, extend satellite lifetimes, and improve mission success rates.

As the field of satellite technology continues to advance, further research in MILP-MPC for GEO satellite station-keeping holds great potential directions. For instance, the MILP formulation can incorporate additional constraints or objectives, such as minimizing communication link disruptions or optimizing satellite attitude control. Moreover, alternative optimization techniques or robust MPC strategies could handle the system uncertainties, e.g., tube-MPC. Furthermore, incorporating machine learning algorithms could enhance the system's adaptability and efficiency. Thus, it utilizes the available real-time telemetry data and advanced disturbance models.

CRediT authorship contribution statement

Mohamed Karim: Writing – review & editing, Writing – original draft, Software, Methodology, Investigation, Formal analysis. **Mohamed Ibrahim:** Writing – review & editing, Software, Resources, Methodology, Formal analysis, Data curation, Conceptualization. **Hosam Hendy:** Writing – review & editing, Supervision, Project administration, Investigation, Formal analysis. **Mahmoud Ashry:** Visualization, Investigation, Formal analysis, Data curation. **Yehia Z. Elhalwagy:** Project administration, Investigation, Funding acquisition.

Declaration of competing interest

The authors declare that they have no conflicts of interest related to this research. The current study was conducted impartially, without any external influence or financial considerations that could potentially bias the results or interpretation.

Acknowledgement

The current work is funded by a joint project (EATA-MTC Micro and Cubesat Mega Project) between the Military Technical College (MTC) and the Science and Technology Development Fund (STDF), the Academy of Scientific Research and Technology (ASRT), and the National Telecommunication Regulatory Authority (NTRA) projects' funding authorities.

Appendix A. Supplemental tables

Table 1
Inclination components ($\mathbb{I}_\tau$, $\mathbb{I}_n$) in the south maneuver.

Cycle number	EOEs	Initial	Reference	Real system	Proposed system
Cycle 1	$\mathbb{I}_\tau$ (rad)	7.71-04	8.37e-04	8.37e-04	8.36e-04
	$\mathbb{I}_n$ (rad)	-1.15e-05	-6.41e-04	-6.29e-04	-6.13e-04
Cycle 2	$\mathbb{I}_\tau$ (rad)	0.00094	0.0010	0.0010	0.0010
	$\mathbb{I}_n$ (rad)	-5.35e-05	-6.72e-04	-6.49e-04	-6.42e-04
Cycle 3	$\mathbb{I}_\tau$ (rad)	0.0012	1.26e-04	1.26e-04	1.26e-04
	$\mathbb{I}_n$ (rad)	1.6e-04	-4.6e-04	-5.01e-04	-4.3e-04
Cycle 4	$\mathbb{I}_\tau$ (rad)	0.0012	1.305e-04	1.31e-04	1.302-04
	$\mathbb{I}_n$ (rad)	2.8e-04	-2.55e-04	-2.61e-04	-2.27e-04
Cycle 5	$\mathbb{I}_\tau$ (rad)	0.0011	0.001176	0.0012	0.0012
	$\mathbb{I}_n$ (rad)	4.38e-04	-1.7e-04	-1.8e-04	-1.4e-04
Cycle 6	$\mathbb{I}_\tau$ (rad)	0.00011	0.0011	0.0011	0.0011
	$\mathbb{I}_n$ (rad)	6.08e-04	-7.5e-06	-1.7e-06	-2.1e-06
Cycle 7	$\mathbb{I}_\tau$ (rad)	7.3-04	7.83e-04	7.94e-04	7.92e-04
	$\mathbb{I}_n$ (rad)	5.4e-04	-0.995e-06	-1.50e-06	-1.9e-06
Cycle 8	$\mathbb{I}_\tau$ (rad)	5.71-04	6.40e-04	6.40e-04	6.38e-04
	$\mathbb{I}_n$ (rad)	4.6e-05	-1.73e-04	-1.58e-04	-1.45e-04
Cycle 9	$\mathbb{I}_\tau$ (rad)	5.51-04	6.07-04	6.1-04	6.1e-04
	$\mathbb{I}_n$ (rad)	3.8e-04	-2.96e-04	-2.43e-04	-2.67e-04
Cycle 10	$\mathbb{I}_\tau$ (rad)	0.00055	0.000595	0.000617	0.000612
	$\mathbb{I}_n$ (rad)	0.00014	-0.000513	-0.00052	-0.00048

Table 2
Eccentricity components ($\mathbb{e}_\tau$, $\mathbb{e}_n$) and semi-major axis ($\mathbb{a}$) in the east maneuver.

Cycle number	EOEs	Initial	Reference	Real system	Proposed system
Cycle 1	$\mathbb{e}_\tau$	0.000117	1.54e-04	1.54e-04	1.47e-04
	$\mathbb{e}_n$	0.000126	1.06e-04	1.06e-04	1.03e-04
	$\mathbb{a}$ (Km)	42164.1	42165.8	42165.8	42165.7
Cycle 2	$\mathbb{e}_\tau$	0.000042	7.3e-05	7.3e-05	6.64e-05
	$\mathbb{e}_n$	0.000226	2.1e-04	2.12e-04	2.07e-04
	$\mathbb{a}$ (Km)	42163.9	42165.29	42165.28	42165.16
Cycle 3	$\mathbb{e}_\tau$	-0.000089	-6.4e-05	-6.5e-05	-6.7e-05
	$\mathbb{e}_n$	0.000253	2.45e-04	2.48e-04	2.44e-04
	$\mathbb{a}$ (Km)	42164.1	42165.16	42165.15	42165.09
Cycle 4	$\mathbb{e}_\tau$	-0.000137	-8.1e-05	-8.1e-05	-8.6e-05
	$\mathbb{e}_n$	0.000178	1.74e-04	1.74e-04	1.69e-04
	$\mathbb{a}$ (Km)	42163.5	42165.8	42165.8	42165.7
Cycle 5	$\mathbb{e}_\tau$	-0.000193	-1.49e-04	-1.48e-04	-1.52e-04
	$\mathbb{e}_n$	0.000232	2.36e-04	2.36e-04	2.27e-04
	$\mathbb{a}$ (Km)	42163.8	42165.7	42165.69	42165.55
Cycle 6	$\mathbb{e}_\tau$	-0.000221	-1.62e-04	-1.58e-04	-1.62e-04
	$\mathbb{e}_n$	0.000108	1.26e-04	1.28e-04	1.23e-04
	$\mathbb{e}_a$ (Km)	42163.2	42165.98	42165.96	42165.79
Cycle 7	$\mathbb{e}_\tau$	-0.000268	-2.24e-04	-2.22e-04	-2.23e-04
	$\mathbb{e}_n$	0.000004	4.5e-05	4.4e-05	3.7e-05
	$\mathbb{a}$ (Km)	42163.4	42165.99	42165.98	42165.8
Cycle 8	$\mathbb{e}_\tau$	-0.000289	-2.57e-04	-2.57e-04	-2.55e-04
	$\mathbb{e}_\tau$	0.000027	5.5e-05	5.6e-05	4.6e-05
	$\mathbb{a}$ (Km)	42163.9	42165.7	42165.7	42165.5
Cycle 9	$\mathbb{e}_\tau$	-0.000274	-2.41e-04	-2.41e-04	-2.41e-04
	$\mathbb{e}_n$	-0.000084	-4.8e-05	-4.7e-05	-5.6e-05
	$\mathbb{a}$ (Km)	42163.9	42165.97	42165.96	42165.77
Cycle 10	$\mathbb{e}_\tau$	-0.000278	-2.49e-04	-2.5e-04	-2.47e-04
	$\mathbb{e}_n$	-0.000068	-3.6e-05	-3.7e-05	-4.6e-05
	$\mathbb{a}$ (Km)	42164.1	42165.87	42165.87	42165.7

Table 3
Eccentricity components (e_x, e_n) and semi-major axis (a) of the collision avoidance maneuver.

Maneuver Type	EOEs	Initial	Reference	Achieved
West Maneuver	e_x	0.00001	0.00003	0.00001
	e_n	0.00015	1.7e-04	1.3e-04
	a (Km)	42164.6	42163.3	42163.4
East Maneuver	e_x	0.000032	0	0.00005
	e_n	0.000185	1.7e-04	2e-04
	a (Km)	42162.9	42164.4	42164.24

Table 4
RMSE of the reference values versus the real system and the reference values versus the proposed system.

Maneuver Type	RMSE (Ref. Vs Real)	RMSE (Ref. Vs Proposed)
South (inclination)	1.49E-05	1.64E-05
East (eccentricity)	1.48E-06	5.42E-06

Table 5
Total firing thruster time for station-keeping maneuvers in seconds.

Cycle no.	Maneuver Type	Real Time(sec)	Proposed Time(sec)	Diff.
Cycle 1	South	666.773	627.587	39.186
	East	28.117	26.8212	1.2958
Cycle 2	South	642.364	613.172	29.192
	East	22.946	19.0722	3.8738
Cycle 3	South	722.389	621.278	101.1
	East	17.1	15.729	1.371
Cycle 4	South	593.023	530.6	62.423
	East	38.648	37.66	0.988
Cycle 5	South	682.81	600.95	81.86
	East	30.687	26.5524	4.1346
Cycle 6	South	659.615	609.53	50.085
	East	45.19	46.9588	-1.7688
Cycle 7	South	600.175	549.5	50.675
	East	41.448	41.7928	-0.3448
Cycle 8	South	685.793	636.286	49.507
	East	29.519	24.2284	5.2906
Cycle 9	South	685.5	675.878	9.622
	East	33.581	30.17	3.411
Cycle 10	South	727.973	646.1	81.873
	East	28.838	23.1952	5.6428
Total Time	Ten Cycles	6982.489	6403.061	579.428

Table 6
Total firing thruster time for collision avoidance (CA) maneuvers in seconds.

Type	Maneuver Type	Real Time(sec)	Proposed Time(sec)	Dif.
CA	West	22.753	19.0750	3.678
	East	22.426	19.8506	2.5754
Total Time	Two maneuvers	45.179	38.9256	6.2534

References

[1] Zou H, Song J, Wang J, Zhang L, Huang Y. Geostationary station keeping using relative orbital elements with model predictive control. In: 2020 Chinese control and decision conference (CCDC). IEEE; 2020. p. 4437–42.
[2] Mancini M, Bloise N, Capello E, Punta E. Sliding mode control techniques and artificial potential field for dynamic collision avoidance in rendezvous maneuvers. IEEE Control Syst Lett 2019;4(2):313–8.
[3] Dutta S, Misra AK. Effect of the nature of uncertainty on the optimization of collision avoidance maneuvers. Adv Space Res 2023;72(10):4132–46.
[4] Hamed AR, Badawy A, Omer AA, Ashry M, Hussein WM. Multiple debris orbital collision avoidance. In: 2019 IEEE aerospace conference. IEEE; 2019. p. 1–8.
[5] De Vittori A, Dani G, Di Lizia P, Armellin R, et al. Numerically efficient low-thrust collision avoidance maneuver design in geo regime with equinoctial orbital elements. In: American astronautical society conference; 2023.
[6] Wang C, Chen D, Liao W, Liang Z. Autonomous obstacle avoidance strategies in the mission of large space debris removal using potential function. Adv Space Res 2023;72(7):2860–73.
[7] Huang X, Yang B, Li S, Wang Z. Efficient high-accuracy North-South station-keeping strategy for geostationary satellites. Sci China, Technol Sci 2021;64(11):2415–26.
[8] Maghsoudi H, Kosari A, Fakoor M, Khoshsima M. A hierarchical fuzzy-optimal strategy for station-keeping maneuver of a geo satellite. IEEE Trans Aerosp Electron Syst 2019;56(3):2212–27.
[9] Sato K, Yoshimura Y, Hanada T, Izumiyama T, Shinohara R. The collision avoidance strategy for geostationary satellites considering orbit maintenance. J Space Saf Eng 2021;8(4):331–8.
[10] Dutta S, Misra AK. Convex optimization of collision avoidance maneuvers in the presence of uncertainty. Acta Astronaut 2022;197:257–68.
[11] Armellin R. Collision avoidance maneuver optimization with a multiple-impulse convex formulation. Acta Astronaut 2021;186:347–62.
[12] Pavanello Z, Pirovano L, Armellin R. Fuel-optimal collision avoidance maneuvers in long-term encounters with station-keeping constraints. Available from: arXiv:2307.06004, 2023.
[13] Liu S, Mu C, Liu Z. Autonomous spacecraft collision avoidance with multiple space debris based on reinforcement learning. In: 2023 42nd Chinese control conference (CCC). IEEE; 2023. p. 2329–34.
[14] Caverly S, Di Cairano Ryan J, Weiss A. On-off quantization of an mpc policy for coupled station keeping, attitude control, and momentum management of geo satellites. In: 2018 European control conference (ECC). IEEE; 2018. p. 1–6.
[15] Zlotnik D, Di Cairano S, Weiss A. Mpc for coupled station keeping, attitude control, and momentum management of geo satellites using on-off electric propulsion. In: 2017 IEEE conference on control technology and applications (CCTA). IEEE; 2017. p. 1835–40.
[16] Weiss A, Kalabić UV, Di Cairano S. Station keeping and momentum management of low-thrust satellites using mpc. Aerosp Sci Technol 2018;76:229–41.
[17] Wijayatunga M, Armellin R, Holt H, Pirovano L, Bombardelli C. Convex optimization-based model predictive control for the guidance of active debris removal transfers. Available from: arXiv:2308.08783, 2023.
[18] Altan A, Hacıoğlu R. Model predictive control of three-axis gimbal system mounted on uav for real-time target tracking under external disturbances. Mech Syst Signal Process 2020;138:106548.
[19] Caverly RJ, Di Cairano S, Weiss A. Split-horizon mpc for coupled station keeping, attitude control, and momentum management of geo satellites using electric propulsion. In: 2018 annual American control conference (ACC). IEEE; 2018. p. 652–7.
[20] Caverly RJ, Di Cairano S, Weiss A. Electric satellite station keeping, attitude control, and momentum management by mpc. IEEE Trans Control Syst Technol 2020;29(4):1475–89.
[21] Gazzino C, Louembet C, Arzelier D, Jozefowiez N, Losa D, Pittet C, et al. Integer programming for optimal control of geostationary station keeping of low-thrust satellites. IFAC-PapersOnLine 2017;50(1):8169–74.
[22] Gazzino C, Arzelier D, Louembet C, Cerri L, Pittet C, Losa D. Long-term electric-propulsion geostationary station-keeping via integer programming. J Guid Control Dyn 2019;42(5):976–91.
[23] Gazzino C, Arzelier D, Cerri L, Losa D, Louembet C, Pittet C. A three-step decomposition method for solving the minimum-fuel geostationary station keeping of satellites equipped with electric propulsion. Acta Astronaut 2019;158:12–22.
[24] Ashraf M, Hendy H, Sallam A, Ashry M, Elhalwagy Y. Modeling and analysis for reaction control thruster used for station-keeping maneuvers of a geo satellite. J Phys Conf Ser 2023;2616:012026.
[25] Karim M, Hendy H, Ashry M, Elhalwagy YZ. Modeling and analysis of orbit determination of geostationary satellites-based on active maneuvers. In: 2024 international telecommunications conference (ITC-Egypt). IEEE; 2024. p. 66–71.
[26] Vallado D, Crawford P, Hujsak R, Kelso T. Revisiting spacetrack report# 3. In: AIAA/AAS astrodynamics specialist conference and exhibit; 2006. p. 6753.
[27] Losa D. High vs low thrust station keeping maneuver planning for geostationary satellites. PhD thesis. École Nationale Supérieure des Mines de Paris; 2007.
[28] Montenbruck O, Gill E. Models, methods, and applications. In: Satellite orbits. Springer; 2014. p. 293–318.
[29] Vallado D. Fundamentals of astrodynamics and applications, Ed. Wertz J.; 2013.
[30] Arefkhani H, Sadati SH, Shahravi M. Satellite attitude control using a novel constrained magnetic linear quadratic regulator. Control Eng Pract 2020;101:104466.
[31] Chobotov VA. Orbital mechanics. third edition; 2002.
[32] Baù G, Hernando-Ayuso J, Bombardelli C. A generalization of the equinoctial orbital elements. Celest Mech Dyn Astron 2021;133:1–29.
[33] Xie Y, Lei Y, Guo J, Meng B. Spacecraft dynamics and control. Springer; 2022.
[34] Ibrahim M, Kögel M, Kallies C, Findeisen R. Contract-based hierarchical model predictive control and planning for autonomous vehicle. IFAC-PapersOnLine 2020;53(2):15758–64.
[35] Findeisen R. Nonlinear model predictive control: a sampled data feedback perspective. PhD thesis. University of Stuttgart; 2006.
[36] Löfberg J. YALMIP: a toolbox for modeling and optimization in MATLAB. In: Proc IEEE Int Symp Comp Aided Cont Syst Design. IEEE; 2004. p. 284–9.
[37] Gurobi Optimization, LLC. Gurobi optimizer reference manual. Available from: https://www.gurobi.com, 2022.